IEEE Access
Multidisciplinary | Rapid Review | Open Access Journal

Received October 7, 2021, accepted October 25, 2021, date of publication November 18, 2021,
date of current version December 15, 2021.

Digital Object Identifier 10.1109/ACCESS.2021.3129319

Direct and Extended Piezoresistive and Piezoelectric Strain Fusion for a Wide Band PVDF/MWCNT-Based 3D Force Sensor

AHMED ALOTAIBI[1,2] AND SOHEL ANWAR[3], (Member, IEEE)
[1]School of Mechanical Engineering, Purdue University, West Lafayette, IN 47906, USA
[2]Mechanical Engineering Department, Taif University, Taif 26571, Saudi Arabia
[3]Department of Mechanical and Energy Engineering, Indiana University–Purdue University Indianapolis, Indianapolis, IN 46202, USA

Corresponding author: Sohel Anwar (soanwar@iupui.edu)

The work of Sohel Anwar was supported by the research fund of Mechatronics and Autonomous Research Laboratory.

ABSTRACT This paper presents a novel 3D force sensor design based on in-situ nanocomposite strain sensors. The polymer matrix of the polyvinylidene fluoride (PVDF) and multi-walled carbon nanotubes (MWCNT) conductive filler nanocomposite film have been chosen as sensing elements for the 3D force sensor. A bioinspired tree branch design was used as the 3D force sensor's elastic structure, that was built using thin Aluminum plates and a laser cutting fabrication process. The PVDF/MWCNT films contained piezoresistive and piezoelectric characteristics, allowing for static/low and dynamic strain measurements, respectively. Two compositions with 0.1 and 2 wt.% PVDF/MWCNT sensing elements were selected for piezoelectric and piezoresistive strain measurements, respectively. These characteristic measurements were investigated under different loading frequencies in a simply supported beam experiment. The 3D force sensor was tested under dynamic excitation in the Z-direction and the X-direction. A Direct Piezoresistive/Piezoelectric fusion (DPPF) method was developed by fusing the piezoresistive and piezoelectric measurements at a given frequency that overcomes the limited frequency ranges of each of the strain sensor characteristics. The DPPF method is based on a fuzzy inference system (FIS) which is constructed and tuned using the subtractive clustering technique. Different nonlinear Hammerstein-Wiener (nlhw) models were used to estimate the actual strain from piezoresistive and piezoelectric measurements at the 3D force sensor. In addition, an Extended direct Piezoresistive/Piezoelectric fusion (EPPF) algorithm is introduced to enhance the DPPF method via performing the fusion in a range of frequencies instead of a particular one. The DPPF and EPPF methods were implemented on the 3D force sensor data, and the developed fusion algorithms were tested on the new 3D force sensor via experimental data. The simulation results show that the proposed fusion methods have been effective in achieving lower Root Mean Square Error (RMSE) in the estimated strain than those obtained from the tuned nlhw models at different operating frequencies.

INDEX TERMS DPPF, EPPF, frequency band, fusion, fuzzy logic, nanocomposite, piezoelectric, piezoresistive, strain sensor, wideband.

I. INTRODUCTION

3D force sensors are essential in many robotic, medical, and machining applications for quantifying the three axial forces simultaneously. These applications include task monitoring, excessive force prevention, and precision placement. Therefore, they have many uses in the field of robot manipulation [1], surgical robots [2], machining applications [3]. 3D force sensors typically consist of elastic structure and sensing elements, which quantify the strain at the elastic structure. Both elements significantly influence the sensor performance and criteria [4]. In addition, cross-coupling between axes' measurements is a limitation that affects the sensor. Several mechanical and bioinspired structures were utilized for the 3D force sensors, such as cross beam [5], parallel mechanism [6] and Stewart platform [7], and tree branches [8]. Some structure configurations could minimize the cross-coupling and improve the sensor performance despite the complex structure and expensive material they are made with [9].

The associate editor coordinating the review of this manuscript and approving it for publication was Yingxiang Liu.

Various sensing elements and approaches have been utilized to quantify strain distributions or deflections on the 3D force sensor structures. These sensing elements are strain gauge [10], Lead zirconate titanate (PZT) [11], optoelectronic [12], and capacitive [13] sensors. Strain gauges and PZT are among the most widely used due to their availability in different sizes and for various environments and are easy to install for different applications. Recently, polymer nanocomposites (PNCs) have received much attention for different strain, force, and pressure measurement applications. These sensors come in flexible matt form or in-situ sensing elements attached to a mechanical structure.

The PVDF-based transducers have been implemented at different applications. In the vibration measurements field, PVDF nanofibers were fabricated using the electrospinning technique [14]. The developed sensing elements captured the operating frequency and applied strain on an experimental cantilever setup. In the gas sensor applications, a fixable PANI/PVDF film sensor was introduced to quantify the ammonia (NH_3) gas level, which is considered a toxic industrial gas [15]. Also, an active stretchable PVDF based on piezoelectric characteristics was constructed for multiple dynamic monitoring applications [16]. The sensor can detect joint motions and vibrations.

Kim. *et al.* [17] proposed a novel multiaxial force sensor; their structure and PNC sensing elements were fabricated using fused deposition modeling (FDM) 3D printing technology. The structure and strain sensor was made of thermoplastic polyurethane (TPU) filament carbon nanotube (CNT)/TPU nanocomposite filament. The strain sensor used the piezoresistive characteristic, which relies on the resistance change at each axis. A 2D micromachined strain sensor was introduced by Su *et al.* [18], which is based on piezoresistivity measurements. The single-walled and multi-walled carbon nanotubes (MWCNTs) were deposited on suspended cantilever beams as strain sensors. For machining applications, a multi-axis dynamometer system was developed using MWCNT/PVDF films [19]. The films were sandwiched between dynamometer structure plates, and the change in voltage was used to measure the 3D cutting forces.

The MWCNT/PVDF nanocomposite's films contain both piezoresistive and piezoelectric characteristics. That results in a strain sensor capable of measuring in static and dynamic loading, respectively. A lower percentage of CNTs inside polymer nanocomposite improves the electrical conductivity of the overall composite [20]. In addition, they can be more sensitive than other conventional strain gauges [21]. Three parameters affected the PNC-CNT's piezoresistivity, and these factors are tunneling, CNTs' crossing, and the resistance of the CNT's itself [22]. In terms of PNC-CNT's conductivity, tunneling resistance is the most dominant parameter [23], while the CNT's resistance has a minor effect [24]. The PVDF is a semi-crystalline polymer with noticeable ferroelectric characteristics, a significant piezoelectric coefficient, and electrical response [25]. It can transform a mechanical loading into an electrical charge and vice versa. These properties allow MWCNT/PVDF nanocomposite's films to be implemented in different piezoresistive or piezoelectric sensing applications.

Various approaches have been proposed to fuse the MWCNT/PVDF sensor's piezoresistive and piezoelectric measurement to achieve a wide band strain measurement. Several researchers combine both characteristics using a multilayered flexible structure for tactile and pressure sensing applications [26], [27]. Even though these sensors have piezoresistive and piezoelectric layers, signal-level fusion was not proved. An optimum linear smoother-based fusion method was proposed to combine the MWCNT/PVDF strain's measurements [28]. The piezoresistive and piezoelectric signals, covariance, and calibration coefficients were utilized to estimate the final fused strain measurement. The calibration coefficients were fixed during the operation frequency bands. This assumption might lead to losing available measurements at some operation frequencies. A novel weighted fusion technique was recently introduced to combine the MWCNT/PVDF strain sensor's piezoresistive and piezoelectric characteristics [29]. The error-based piezoresistive piezoelectric fusion (PPF) is based on fuzzy logic (FL), where data-driven approaches were used to generate the PPF's fuzzy inference system (FIS). These approaches were optimization method, fuzzy c-means (FCM) clustering, subtractive clustering, and combination of type-2 fuzzy and subtractive clustering. This methodology has achieved better fusion performance and minimum Root Mean Squared Errors (RMSEs) than other fusion approaches at different operating frequencies.

This paper presents a novel 3D force sensor using the MWCNT/PVDF strain sensor films and bio-inspired structure configuration. The sensing elements were fabricated using a spray coating process. A direct PPF method was implemented to fuse piezoresistive and piezoelectric characteristics using strain measurements at a specific operating frequency. The PPF method was enhanced by adding the operation frequency data into the FIS, which allows a single FIS to operate at a specific operating frequency. The extended PPF (EPPF) was introduced to allow fusion at a range of frequencies instead of a specific operating frequency at the DPPF. The MWCNT/PVDF strain sensor's measurements were analyzed at different frequencies using a cantilever beam under dynamic loading. In addition, the 3D force sensor was tested under Z and X axes dynamic loading using specific fixtures. The DPPF was performed on all 3D force sensor's beams, while the EPPF was tested on the positive beams at the X and Y axes.

II. NANOCOMPOSITE STRAIN SENSOR FABRICATION

The 3D force sensor manufacturing process involved sensing element fabrication and 3D structure machining. The PNC's solutions preparation and film fabrication procedure are discussed in the following section. In addition, the selected 3D force sensor's structure configuration machining and NC

sensing elements assemble were presented in the following subsections.

A. PVDF/MWCNT FILM FABRICATION

Polyvinylidene Fluoride (PVDF) was chosen as the matrix host for the nanocomposite sensor because of its high piezoelectricity characteristic. The 0.1 wt.% and 2 wt.% MWCNT/PVDF nanocomposites have been chosen due to their optimal performance for piezoelectric and piezoresistive measurements, respectively [28]. The PVDF powder was purchased from Sigma Aldrich. The average molecular weight (Mw) of the powder was approximately 534,000 mol wt. The Multi-Walled Carbon Nanotubes (MWCNTs) were used as nano conductive fillers for the strain sensor. The MWCNT was purchased from Sigma Aldrich, and their outer diameter and their length were 7-15 nm, and 0.5-10 μm, respectively. The film was fabricated using a solution mixing process followed by a spray-coating technique described in the literature [28]. First, the PVDF was fully dissolved in N-N dimethylformamide (DMF) and stirred on a hot plate for 3 hrs at a temperature of 80 °C. Then, different concentration of MWCNT was mixed with DMF, and the solution was sonicated for 30 min at room temperature until full desperation of the mixture was achieved. The two sensors were fabricated using the MWCNTs, PVDF, and DMF's percentages and weights are shown in Table 1.

TABLE 1. The MWCNTs, PVDF and DMF's concentrations for each sensor.

	1st solution		*2nd solution*	
%wt	PVDF(g)	DMF (ml)	MWCNT (g)	DMF (ml)
0.1	4	40	0.004	10
2	1	10	0.02	50

The percentage of PVDF to DMF was 0.1 g/mL in the 1st solution, whereas the percentage of the MWCNT to the DMF was 0.0004 g/mL. Then, the two solutions were mixed at room temperature and stirred for one hour. Spray-coating, which produces random MWCNT dispersion, was selected to fabricate the proposed sensors. An airbrush was used to manually spray the PVDF/MWCNT solution mix on glass substrates, as shown in Fig. 1.

The PVDF/MWCNT solution was poured inside the air brush's color cup and sprayed in a zig-zag path for about 144 and 330 rounds for the 0.1 wt.% and 2 wt.% MWCNT/PVDF films. Each spray round traveled from left to right and then from up to dawn, respectively, until the whole substrate was covered with nanocomposite droplets. Each deposited layer was air-dried using air between rounds. The sprayed films on the substrates were then placed on a hot plate at 80 °C until all of the solvent is evaporated. Then, they were placed in a sonication container for a few minutes to peel the film off the glass substrates. These fabrication processes for the PVDF/MWCNT film sensor using solution mixing and spray coating are summarized in Fig. 2.

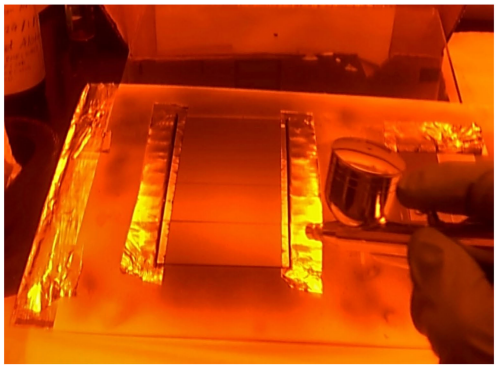

FIGURE 1. Spray coating process of 2 wt.% MWCNT/PVDF film.

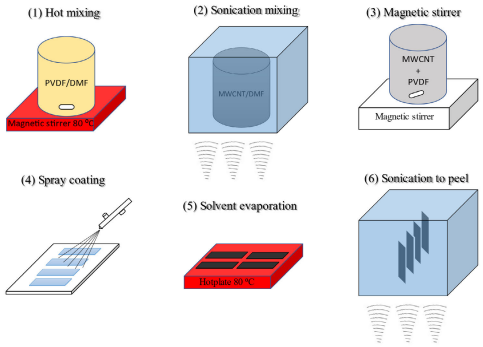

FIGURE 2. Fabrication processes of the PVDF/MWCNT films using spray-coating.

Afterward, the films were removed from their substrates and taken out of the sonication container, the nanocomposite films were easily removed out of the substrate by hand, as shown in Fig. 3. The thicknesses of the fabricated films with the two different concentrations were then measured. The average thickness of the 0.1 wt.% and 2 wt.% films were 40 and 25 μm, respectively.

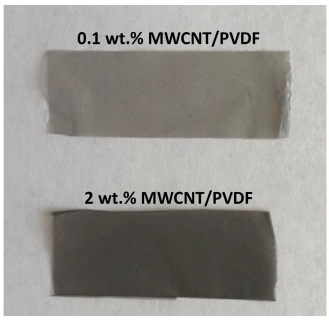

FIGURE 3. The fabricated PVDF/MWCNT film.

B. 3D FORCE SENSOR FABRICATION

The structure configuration is a critical parameter that influences the 3D force sensor's performance. Different bio-inspired structures were proposed for the 3D force's structure

and analyzed for their structural sensitivity and measurement coupling [8]. The tree branch structure was found to have achieved lower coupling characteristics between strain measurements [8]. As a result, the tree branch design was selected to produce the proposed 3D force sensor. The 3D force sensor's structure was made of Aluminum (Al) with a thickness of 1.6 mm and fabricated using laser cutting technology, as shown in Fig. 4.

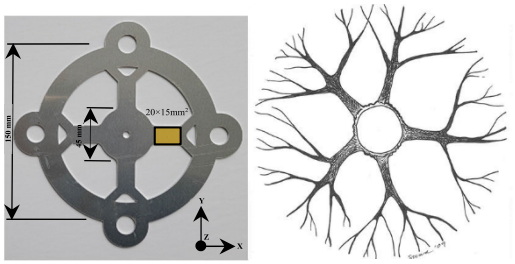

FIGURE 4. The 3D force's (a) leaser cut structure; and (b) Tree branches' top view [30].

The structure consisted of an inner ring, an outer ring, and four connecting beams. The rings are connected with four beams. Generally, the 3D forces are applied to the center of the structure. A bolt hole was inserted in the structure's center. For mounting purposes, four bolt holes were open at the end of each beam along the outer ring's circumference.

The sprayed 0.1wt.% and 2wt.% MWCNT/PVDF films were retrieved to quantify the strain on the 3D force's structure using their piezoelectric and piezoresistive characteristics. The sensing element installment and connections are shown in Fig. 5. First, four films of each concentration were cut down from the same sprayed films. All films had the same dimension of approximately 5 × 25 mm. Then, one of each 0.1wt.% and 2wt.% MWCNT/PVDF films were put into four groups and attached in parallel to a single double-sided Kapton tape using the tape adhesion. On the Kapton tape, both sensing elements were separated by a distance of approximately 2 mm. Next, four commercially available strain gauges were attached to the bottom side of the 3D force sensor in the middle of each beam. The strain gauges were assumed to measure the same strain measured by the NC films, with the same magnitude and opposite phase. Later, the Kapton tapes, including the sensing elements, were attached to the centers of the four beams of the 3D force sensor. Lastly, silver epoxy was used as electrodes for the MWCNT/PVDF films and the electrical wires' connections for measuring the strains.

III. EXPERIMENTAL SETUP

The fabricated MWCNT/PVDF sensors' and 3D force sensor's performance were analyzed and tested using different experimental setups. Additionally, the piezoresistive and piezoelectric strain measurements' characteristics were tested using a cantilever vibration beam setup. Finally, the 3D force sensor performance and fusion were conducted using a 3D force vibration setup. The following subsection discusses both methodologies.

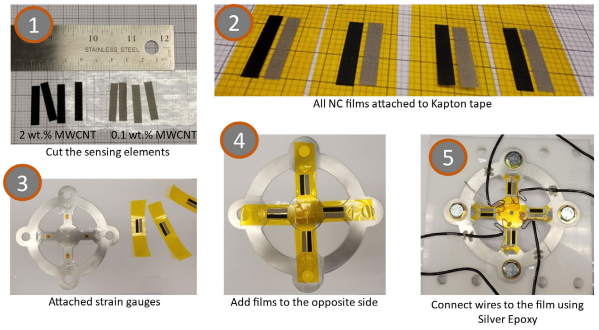

FIGURE 5. The 3D force sensing element's attachment and connection process.

A. CANTLIVER VIBRATION TESTING SETUP

The cantilever vibration beam setup was constructed using B&K vibration exciter Type 4808 and Al beam, as shown in Fig. 6. The first end of the beam was attached to a fixed end, while the other end was connected to the shaker. A 0.1wt.% film and 2wt.% MWCNT/PVDF films and a strain gauge were attached close to the fixed end, where higher strain measurements were expected. Wires were connected to the NC films using silver epoxy, which acted as the sensing elements' electrodes. The beam was excited at 0.5 Hz, 1 Hz, 5 Hz, 10 Hz, 50 Hz, 100, and 1000 Hz vibration frequencies. The Fast Fourier Transform (FFT) was applied to both measurements' signals using the (signal-to-noise ratio) SNR command in MATLAB to analyze the piezoresistive and piezoelectric strain sensors' characteristics.

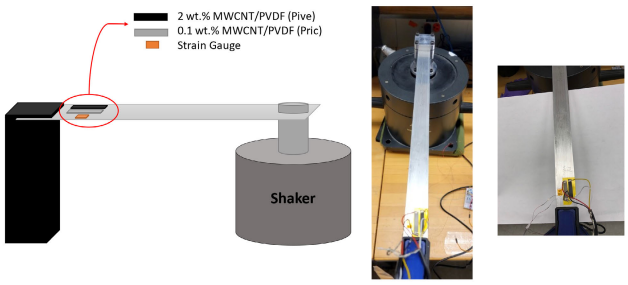

FIGURE 6. The cantilever vibration beam setup.

B. 3D FORCE SENSOR VIBRATION TESTING SETUP

The 3D force sensor was tested for X-axis and Z-axis' vibrations. For the dynamic loading experiment of the sensor in the Z direction, a fixture was designed to hold the sensor above the vibration exciter, as shown in Fig. 7. The 3D Force sensor was then excited at 2 Hz, 5 Hz, 10 Hz, 100 Hz. The fixture was made off a High-Density Polyethylene (HDPE) sheet with a thickness of 12.7 mm and four threaded rods with nuts. The four threaded rods connected the HDPE sheet and the shaker's

base to make the fixture more rigid. The 3D force sensor was centered and connected to the shaker using a small threaded rode. In addition, four bolts were used to attach the sensor to the HDPE sheet.

(a) (b)

FIGURE 7. The 3D force sensor vibration setup for Z-axis (a) fixture CAD design and (b) actual 3D force sensor attached to the fixture.

For the X-direction dynamic loading experiment, an extra HDPE sheet was inserted perpendicular to the previous sheet for the X dynamic loading experiment, as shown in Fig. 8. Four brackets were used to hold the HDPE sheets. As a result, the 3D force sensor was perpendicular to the shaker. The 3D force sensor and the shaker were connected using threaded rods and a small bracket.

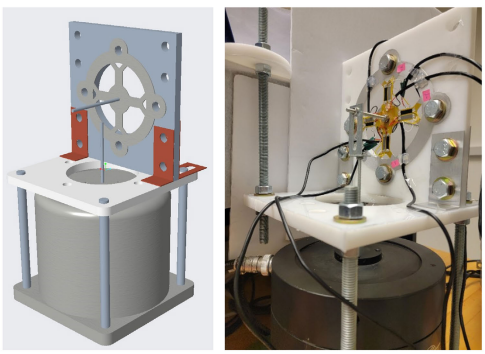

(a) (b)

FIGURE 8. The 3D force sensor vibration setup for X-axis (a) fixture CAD design; and (b) actual 3D force sensor attached to the fixture.

C. PIZORESISTIVE AND PIEZOELECTRIC CIRCUITS AND ACQUISITION SYSTEM

The MWCNT/PVDF film's resistance change represents the piezoresistive characteristics, while the film's generated charge characterizes the piezoelectric measurement. The Wheatstone bridge was used to magnify the resistance change for the piezoresistive sensing elements utilizing quarter bridge configuration, as shown in Fig. 9a. The 3D force sensor was tested under different excitation frequencies using the Z-axis and X-axis loading fixtures. At the same time, the piezoresistive sensors, piezoelectric sensors, and strain gauges' measurement were obtained, analyzed, and implemented in the PPF based methods.

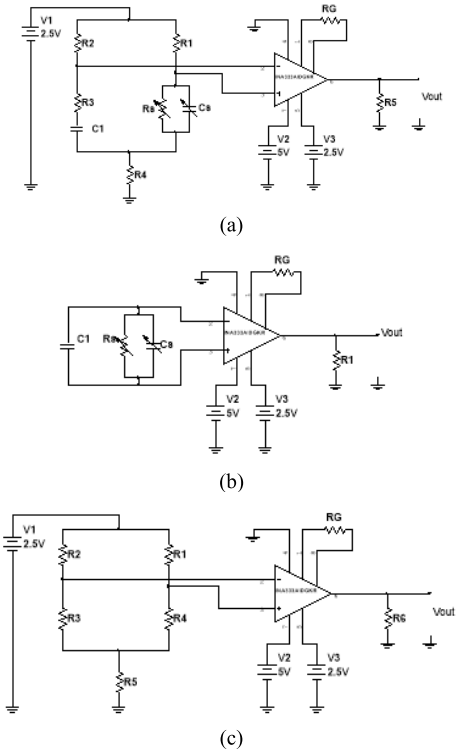

FIGURE 9. Electrical circuits for MWCNT/PVDF's (a) piezoresistive; (b) piezoelectric; and (c) reference strain gauge strain sensors.

The final output voltage (E_o) for the Wheatstone bridge based sensors' circuits can be approximated using Equation (1) [31]:

$$V_{out} = V_i \frac{\delta R/R}{4(1 + R/R_g)} \tag{1}$$

where input voltage (V_i), amplifier internal resistance (R_g), initial bridge resistance (R) assuming all initial bridge resistances are equal, and sensor resistance changes by an amount (δR) are used to calculate the V_{out}. While the capacitive behavior of the piezoresistive circuits was ignored in this Equation. On the other hand, Equation (2) is used to estimate the final output voltage (V_{out}) of the charge amplifier's circuits in terms of the sensor-generated charge (q) and feedback capacitances (C_r), [31]:

$$V_{out} = -q[C_r + (\frac{C_T}{A_0})] \tag{2}$$

where $C_T = C_t + C_c + C_r$ ($\mathbf{C_t}$, $\mathbf{C_c}$, and $\mathbf{C_r}$ representing the transducer, cable, and feedback capacitances), and $\mathbf{A_0}$ is the amplifier open-loop gain. The sensing element has an internal variable resistance ($\mathbf{R_s}$) and capacitance ($\mathbf{C_s}$). A capacitance $\mathbf{C_1}$ was combined with the resistance **R3** to achieve a balanced bridge while ensuring all bridge's resistances were equivalent. The bridge was supplied by 2.5 volts.

The sensing element has an internal variable resistance (R_s) and capacitance (C_s). A capacitance C_1 was combined with the resistance R3 to achieve a balanced bridge while ensuring that all the bridge's resistances were equivalent. The bridge was then supplied with 2.5 volts. The instrumentation amplifier INA333 from Texas Instruments was selected for the piezoresistive, piezoelectric, and reference strain gauge circuits. The INA333 is considered to be a precise and low-power amplifier for high-accuracy applications [32]. The amplifiers were powered by 5 volts, and a reference voltage of 2.5 volts was provided using the precision series voltage reference REF5025 from Texas Instruments [33]. The gain-setting resistor (RG) was used to assign the desired measurement amplification gains. For piezoelectric measurements, the 0.1 wt.% MWCNT/PVDF film was connected in parallel with a capacitor C1. A similar circuit has been used in different pressure sensing applications and proven its effectiveness [34]. A quarter Wheatstone bridge was used for the strain gauge measurement similar to the piezoresistive circuit, except no capacitance was inserted on the bridge. This is because of the approximately purely resistive behavior of strain gauges compared to MWCNT/PVDF sensor.

The outputs of the instrumentation amplifiers were sent to LABVIEW using data acquisition cards (DAQs) from National Instruments (NI). The strain gauges were calibrated using the gauge factors. Then, the calibrated strain gauges were used to calibrate both piezoresistive and piezoelectric measurements at each beam individually. Band bass filter was used to filter all measurements of the 3D force sensor. Both the DPPF and the EPPF used the calibrated strain measurements from piezoresistive, piezoelectric, and strain gauges during the learning, tuning, and testing of the 3D force sensor fusion.

IV. PIEZORESISTIVE/PIEZOELECTRIC FUSION (PPF) METHODS

A. THE DIRECT PPF METHOD

The direct PPF method was proposed to combine the piezoresistive and piezoelectric element's measurements of the MWCNT/PVDF strain sensors using a fuzzy logic-based methodology, as shown in Fig.10. The piezoresistive and piezoelectric element's measurements are used by the DPPF's FIS as input variables for the DPPF's FIS. Compared to the original PPF method used in the study [29], the direct PPF utilized the piezoresistive and piezoelectric measurements instead of their estimated errors.

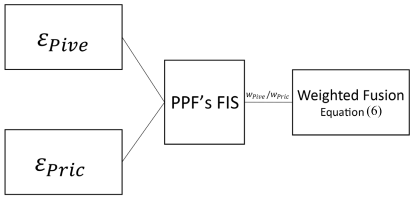

FIGURE 10. Schematic of the direct piezoresistive/piezoelectric fusion (DPPF) method.

The FIS determines the piezoresistive weight ($\boldsymbol{w_{Pive}}$) or piezoelectric weight ($\boldsymbol{w_{Pric}}$) based on both the measurements and the FIS's structure and configuration. The final fused strain signal ($\boldsymbol{\varepsilon_f}$) was calculated using Equation (3) [29], as follows:

$$\varepsilon_f\,(k) = w_{Pive}\,(k)\,\varepsilon_{Pive}\,(k) + w_{Pric}\,(k)\,\varepsilon_{Pric}\,(k) \tag{3}$$

where the piezoresistive strain ($\boldsymbol{\varepsilon_{Pive}}$) and piezoelectric strain ($\boldsymbol{\varepsilon_{Pric}}$) contribution to the final fused strain measurement are determined by the assigned weights, which are $\boldsymbol{w_{Pive}}$ and $\boldsymbol{w_{Pric}}$, respectively. The weights span the values from zero to one depending on the sensitivity of the piezoresistive and piezoelectric measurement at that frequency. This Equation has an infinite amount of solutions due to the presence of the two unknown weighting factors in a single fusion equation. Consequently, one of the sensors was assigned a total weight of one while the other sensor's weight was estimated using the following Equations (4) or (5) [29]:

$$\boldsymbol{w_{Pive}} = \frac{\boldsymbol{\varepsilon_{act}} - \boldsymbol{w_{Pric}} \times \boldsymbol{\varepsilon_{Pric}}}{\boldsymbol{\varepsilon_{Pive}}} \tag{4}$$

$$\boldsymbol{w_{Pric}} = \frac{\boldsymbol{\varepsilon_{act}} - \boldsymbol{w_{Pive}} \times \boldsymbol{\varepsilon_{Pive}}}{\boldsymbol{\varepsilon_{Pric}}} \tag{5}$$

At low frequencies, the piezoresistive strain sensor has higher accuracy and is more sensitive to strain measurements. On the other hand, piezoelectric sensors outperform the piezoresistive sensors when taking high-frequency strain measurements. Thus, a weight of one was assigned to the piezoresistive sensor at low frequency, while the $\boldsymbol{w_{Pric}}$ calculated using Equation (5). Conversely, the piezoelectric sensor was given a whole weight of one, while the $\boldsymbol{w_{Pive}}$ was calculated using Equation (4). During the data preparation for the DPPF's FIS, all measurements, including the reference strain gauges measurements, were shifted by a positive constant number c to avoid getting infinity weights in the Equations (4) and (5) caused by the harmonic strain measurement and zero-crossing at no strain conditions. The shifted data were used to calculate both weights and the final fused strain equation became [29]:

$$\varepsilon_f\,(k) = w_{Pive} \times (\varepsilon_{Pive} + c) + w_{Pric} \times (\varepsilon_{Pric} + c) - c \tag{6}$$

In this work, to assign either the piezoresistive or piezoelectric weight, the DPPFs FIS goes through three phases. These phases are the fuzzification, rule generation and FIS process, and defuzzification. First, both measurements are mapped to a range of values from the minimum to the maximum strain values using Membership Functions (MFs) representation. The MFs are described using linguistic variables implying the input's or output's characteristics. In the DPPF method, either the piezoresistive or piezoelectric's weight is selected as the FIS's output depending on the operation frequency and strain sensitivity for each measurement characteristic. The Fuzzy Inference System (FIS) converts given fuzzy inputs into outputs depending on a preassigned set of rules [35]. Then, the fuzzy output values are transferred to actual values in the defuzzification phase [35]. In the DPPF

method, the intermixed output is defuzzied to produce the desired piezoresistive or piezoelectric's weights. The Center of Area (COA) method and a weighted average method are used to perform the defuzzification prosses for Mamdani and Sugeno FIS, respectively [36]–[38].

Constructing and tuning the FIS given input/output data is a complex process in the system that contains multiple input/output MFs and rules. In the previous work [29], several data-driven approaches were utilized to produce the DPPF'FIS using Fuzzy Logic and Global Optimization Toolboxes in MATLAB [39]. The method is based on the normalized input errors for both measurements. The reference strain gauge measurements were assumed to be the actual strain values. The subtractive clustering-based PPF systems have achieved very low RMSE compared to the optimization and Fuzzy C-means (FCM) clustering methods [29]. As a result, the subtractive clustering technique was used to generate and tune the FIS's parameters and assign the rule set for the direct PPF's performance. All measurement data and reference strain gauges were shifted by a constant number of one at all operating frequencies. This methodology resulted in a single FIS for each operation and limited the fusion to a single operating frequency.

B. THE EXTENDED PIEZORESISTIVE/PIEZOELECTRIC FUSION (EPPF) METHOD

As discussed in the previous section, the direct PPF method utilizes the piezoresistive and piezoelectric element's measurements to perform the fusion. The fusion is performed at a certain frequency using both measurements and a single FIS that would result in a complex PPF's structure in the case of the strain measurement at a range of operating frequencies. To address this issue, the EPPF method was introduced to minimize the number of FISs and reduce the direct PPF method's complications, as shown in Fig.11.

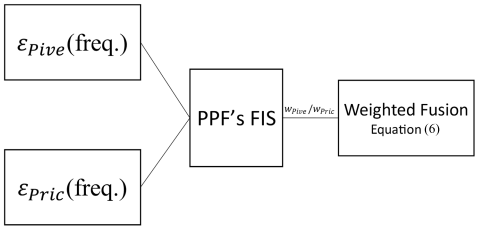

FIGURE 11. Schematic of the extended piezoresistive/piezoelectric fusion (EPPF) method.

In the EPPF method, the measurements of the piezoresistive strain ($\boldsymbol{\varepsilon_{Pive}}$) and piezoelectric strain ($\boldsymbol{\varepsilon_{Pric}}$) taken at different frequencies were cascaded. The cascaded signals data was used to generate and tune the EPPF's FIS, rules, input, and output MFs. In this way, the PPF method's generation approach and the fusion equation were used to produce the EPPF method. In comparison to the DPPF, the EPPF fuses both measurements at the span of frequencies using a single FIS.

C. ACTUAL STRAIN ESTIMATION USING NONLINEAR MODELING

Several researchers have reported the nonlinearity in the CNT-PNC's piezoresistive and piezoelectric characteristics. The current-voltage (I-V) curve was used to assess the composite nonlinearity performance. Ounaies *et al.* [40] investigated the nonlinear performance of the single-walled carbon nanotube (SWCNT)/polyimide composites. The tunneling effect was responsible for nonlinear behavior. Similarly, nonlinearity was observed for the 0.35 wt.% SWCNT/polydimethylsiloxane composite and faded at the 5wt.% composite [41]. For a similar composite, the I-V curve of a 0.2 wt% CNT/epoxy composite was nonlinear and linear at a high concentration of the CNT [42]. The CNT/epoxy composite tunneling resistance at low CNT content and strain level higher than 0.2 % resulted in a nonlinear piezoresistive's performance [43]. In terms of a CNT/polymer's piezoelectricity, an electrospun PVDF nanofibers mat with no CNTs had achieved a linear voltage-weight relationship [44]. However, nonlinearity was apparent at the 0.3 wt. % CNTs composite. Vinogradov *et al.* [45] investigated the PVDF's dynamic response and reported the accelerated creep performance due to the cyclic loading at stress levels below the viscoelastic linearity limit. In these ways, researchers have remarked on the nonlinear piezoresistive and piezoelectric's performance of the CNT-PNCs.

Hammerstein-Wiener models have been used to estimate the actual strain given the input piezoresistive measurement at a low frequency or piezoelectric measurement at higher frequencies. The System Identification Toolbox in MATLAB has been used to construct the Hammerstein-Wiener models. The Hammerstein-Wiener model is used as a black-box model because it does not include the physical perceptiveness of the internal processes [46]. As shown in Fig. 12, the dynamic systems are represented by a discrete linear block and one or two nonlinear memoryless static blocks [46].

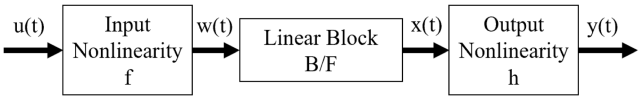

FIGURE 12. Hammerstein-Wiener model's block diagram.

The Hammerstein-Wiener (HW) model has been used for modeling at different sensors and actuators modeling to simulate the nonlinear effect either in input or output of a linear system [46]. Despite being one model, this model comes in three structure configurations, such as the Hammerstein model, the Wiener model, and the linear model. It is called the Hammerstein model if there is no output nonlinearity h block, and it is named the Wiener model if it contains only the linear block and output nonlinearity h block. The nonlinear Hammerstein-Wiener (nlhw) becomes a linear transfer function if both input and output nonlinearities are removed. For a SISO system, the nlhw models are configured using the number of zeros and poles, input and output

nonlinearity estimators, and input delay. In this work, several input/output nonlinearity configurations have been utilized from the system identification toolbox, such as a sigmoid network, a piecewise linear function, and a unit gain (no configuration assigned) [46]. For the DPPF method, a nlhw model was used to estimate the actual strain from either piezoresistive or piezoelectric sensors at a single operating frequency. The DPPF and EPPF's performances were compared with the actual strain measurement and nlhw models.

V. VALIDATION OF THE DPPF AND EPPF METHODS AND RESULTS

The DPPF and EPPF method tested and validated using a Simulink model. The model consisted of both characteristics' measurement, fuzzy logic controller (FL) block, and the fusion equation. The FL system produces the desired weights based on the piezoresistive and piezoelectric measurements. The final fused strain is combusted using Equation (6). The fused strain compared with actual strain gauge and nlhw models' measurements using the RMSE for each.

The piezoresistive and piezoelectric characteristics of the MWCNT/PVDF strain sensor were influenced by the operating frequency. The piezoresistive sensing element was more sensitive at low frequencies, while the piezoelectric sensor was more accurate at higher frequencies [28]. As a result, the DPPF and EPPF were proposed to fuse both measurements at specific frequencies and a range of frequencies, respectively. The performances of both characteristics were investigated using a vibrating cantilever at different frequencies. In addition, a 3D force sensor was fabricated and assembled. The piezoresistive and piezoelectric element's measurements were taken at the elastic beams of the 3D force's structure and were fused using the DPPF and EPPF methods. The subtractive clustering technique was used to generate and tune the proposed methods.

A. CANTILEVER VIBRATION RESULTS

The piezoresistive and piezoelectric element's measurements were investigated using a cantilever beam under different vibration frequencies, as shown in Fig. 6. This experiment was conducted to identify the operating frequencies for each characteristic. Also, these limitations were used to assign weight during the DPPF and EPPF generating processes. Testing was completed under vibrations of 0.5 Hz, 1 Hz, 5 Hz, 10 Hz, 50 Hz, 100 Hz, and 1000 Hz. The FFT results were retrieved for the piezoresistive and piezoelectric element's measurements at these frequencies, as shown in Fig. 13a and Fig.13b. The piezoresistive signals were more sensitive at frequencies 0.5 Hz, 1 Hz, and 5 Hz compared to the piezoelectric measurements. At the 10 Hz excitation, the piezoelectric measurement achieved a slightly higher SNR of 15.99 dB than the piezoresistive signal's SNR of 13.43 dB. The piezoelectric measurement became more apparent and

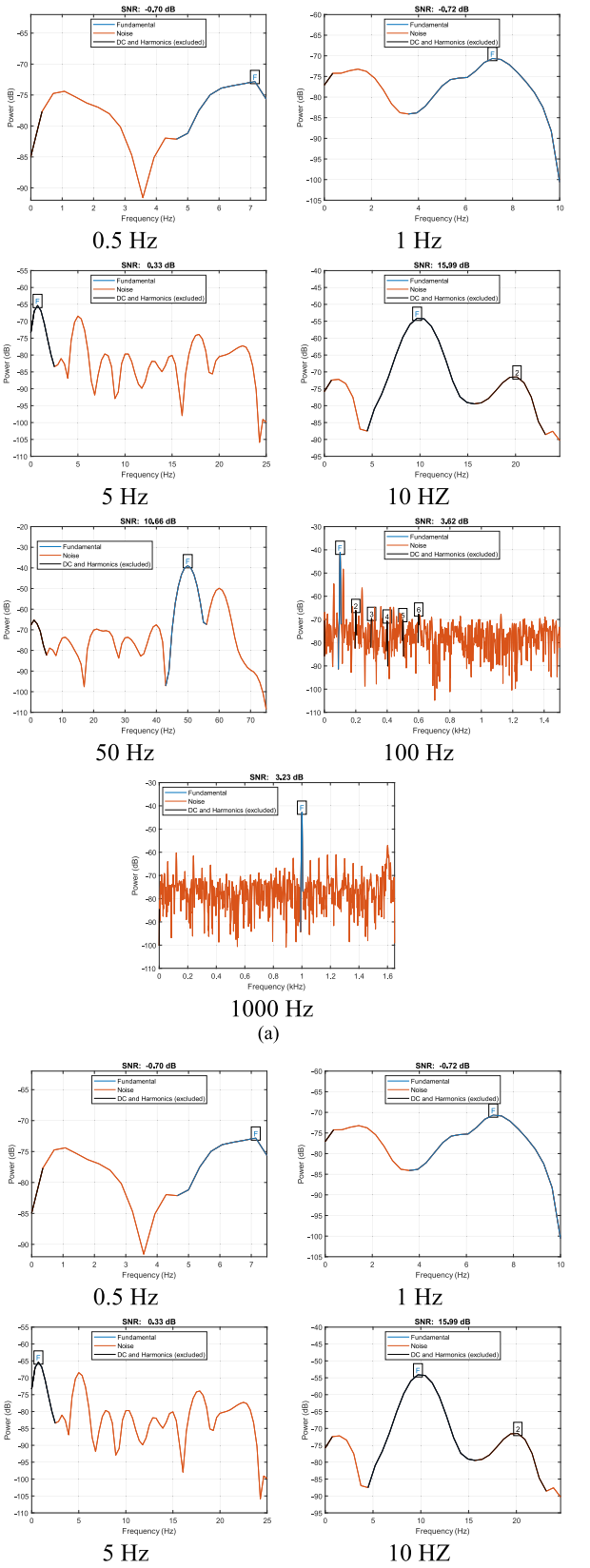

FIGURE 13. a. The piezoelectric measurements' FFT at the cantilever testing setup. b. The piezoresistive measurements' FFT at the cantilever testing setup.

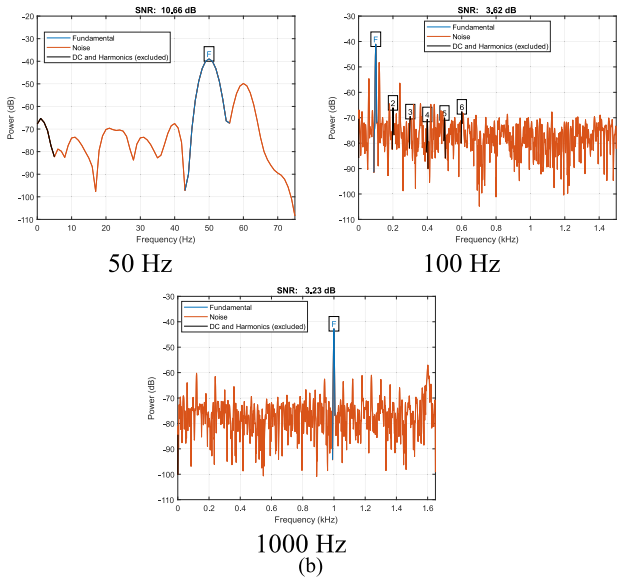

FIGURE 13. *(Continued.)* **b. The piezoresistive measurements' FFT at the cantilever testing setup.**

was not affected by the electric hum, which had a fundamental frequency of 60 Hz. On the other hand, the piezoresistive signal's magnitude was lower, yet it was not affected by the noise.

At 100 Hz, the piezoresistive sensor presented high-frequency noises compared to the piezoelectric sensor. In addition, the piezoelectric sensor was accurate at 1000 Hz, while the piezoresistive sensor underwent large low-frequency noises. As a result, the piezoresistive sensor illustrated good signal characteristics at frequencies below 50 Hz, while the piezoelectric sensor's measurements were less sensitive to noises.

B. 3D FORCE SENSOR VIBRATION RESULTS AND THE DPPF

The 3D force sensor was fabricated and tested for the fusion of strain measurements and characteristics. The cantilever experiment proved the sensitivity of the piezoresistive sensor at lower frequencies. In addition, the piezoelectric sensor showed good sensitivity at frequencies above 50 Hz. As a result, the piezoresistive and piezoelectric measurements were assumed to be accurate at lower and higher frequencies, respectively. However, each type of sensor showed a lower content signal at the other sensor type's accurate measurement frequency. The DPPF utilized the piezoresistive and piezoelectric's measurements to achieve an accurate strain measurement.

The DPPFs' FISs were constructed and tuned using the subtractive clustering technique. Sugeno-based FIS was considered in this study due to its advantage in nonlinear dynamic systems applications [47]. The Gaussian MFs were used for the FISs' input. The Sugeno's FIS produces two values, which are rule output level (z_i) and rule firing strength (w_i) for each i rule [48]. The rule antecedent AND method is used to compute the w_i value, while the output MF z_i is a function in FIS's inputs and constant values a_i, b_i and c_i, as shown in (7):

$$z_i = a_i x + b_i y + c_i \tag{7}$$

For N number of rules, the final output is evaluated using all rules' output using the weighted average method, as shown in (8):

$$Final\ Output = \frac{\sum_{i=1}^{N} w_i z_i}{\sum_{i=1}^{N} w_i} \tag{8}$$

The 3D force sensor was tested at 2 Hz, 5 Hz, and 10 Hz, and 100 Hz under Z-axis and X-axis loading scenarios. At the three lower frequencies, the piezoresistive was assigned the total weight of one, while piezoelectric sensors' weights were computed using Equation (5). At 100 Hz, the piezoelectric sensors' weights were computed using Equation (4), and the weight of one that had been appointed for the piezoresistive sensors. The input MFs, output MF's linear Equation constant, and the rules were generated and tuned using the piezoresistive measurements, piezoelectric measurement, and the computed desired weight. For each FIS, a set of rules was generated to relate the FIS's input and output MFs, as shown in Table 2. Each resultant input membership function consisted of multiple data sets or clusters, where the number of MFs equaled the number of clusters and rules. The same rules table was generated for each FIS except the number of rules (n), which depended on the MF's number.

TABLE 2. **The DPPF'S FISs rules.**

FIS's rules
1. If (in1 is in1cluster1) and (in2 is in2cluster1) then (out1 is out1cluster1)
2. If (in1 is in1cluster2) and (in2 is in2cluster2) then (out1 is out1cluster2)
……
n. If (in1 is in1cluster n) and (in2 is in2cluster n) then (out1 is out1cluster n)

1) Z AXIS LOADING SCENARIO

The resultant FISs' input MFs for the operating frequencies were retrieved from the Z-axis loading test, as shown in Fig. 14 and Fig. 28. Both piezoresistive and piezoelectric strain data have been represented by different numbers of clusters, which are referred to by data and the cluster number. Please refer to the Appendix for the FISs' input MFs at 5 and 10 Hz under Z loading conditions. The 3D force sensor consisted of four beams in the ± X-direction and ±Y-direction. At each frequency, two input variables were assigned for each beam's DPPF's FIS. These input variables were the piezoresistive and piezoelectric element's strain measurements. The input MFs' range spanned the values from the minimum to maximum piezoresistive and piezoelectric element's strain measurements' data. At the same time, the degrees of memberships spanned the values

from zero to one. The number of MFs at each beam and frequency was determined by the number of clusters assigned to represent the relationship between the strain measurements and desired weight by the subtractive clustering method. The cluster influence range was the spatial parameter that decided if an input/output data point was considered part of a specific center group. It was a scalar number ranging from zero to one. In this manner, the number of the MFs assigned by the cluster influence range was defined for each test. For each scenario, the cluster influence range was adjusted manually to achieve the best estimate of the actual strain's estimate with a minimum number of MFs. At least three MFs were utilized by two beams at the excitation of 2 Hz and 5 Hz, as shown in Fig. 14a. At the frequency of 2 Hz, the +Y beam's FIS had the highest number of MFs 2 Hz because of the lower cluster influence range, as shown in Fig. 14a. Only four MFs were utilized for the DPPF's FISs at the four beams under 10 Hz excitation in the Z-direction. Similarly, the input MFs at the beams, which vibrated at 100 Hz, used four MFs of the FIS's input variables except at the +Y beam, as shown in Fig 13b. The four MFs were achieved using a cluster influence range of one.

The rule output level's (z_i) coefficients were generated, and only output MFs of the -X beam under 2 Hz excitation were plotted, as shown in Fig.15. The rest of the outputs MFs at each beam and frequency followed the same process and attained different constant values. The number of outputs' MFs equals the number of clusters, input MFs, and assigned rules in each case. As a result, four output's clusters were generated for the -X beam under the vibration of 2 Hz. 1n the Equation (7), piezoresistive and piezoelectric strain measurements and coefficients assigned by the subtractive clustering method were used to calculate the rule's output level (z_i). In addition, the number of rules was four (n = 4), as shown in Table 2.

The proposed Simulink model was used to test and validate the resultant DPPF's FISs. The FISs used the piezoresistive, and piezoelectric strain measurements as inputs, and the outputs were based on the appropriate operating frequency. The DPPF's fused strains were calculated using Equation (6) and the FIS's output weight. The DPPF's fused strains were retrieved and compared with the measurements' characteristics, measurements from reference strain gauges, and the nlhw model's estimated measurements, as shown in Fig. 16. The DPPF's fused strains agreed closely with the reference strain gauges when the 3D force sensor was excited at the Z-axis. At 10 Hz, the nlhw model's strain estimate was more accurate than the DPPF's fused strains at the -X beam (2 Hz), the +Y beam (2 Hz), and the -Y beam (10 Hz). However, the DPPF method did successfully fuse both measurements and therefore achieved more accurate results.

In this work, different nlhw models were used to estimate the actual strain from either the piezoresistive or the piezoelectric sensors at three lower frequencies and 100 Hz, respectively. The MATLAB's system identification toolbox was used to produce the best fit actual strain estimate.

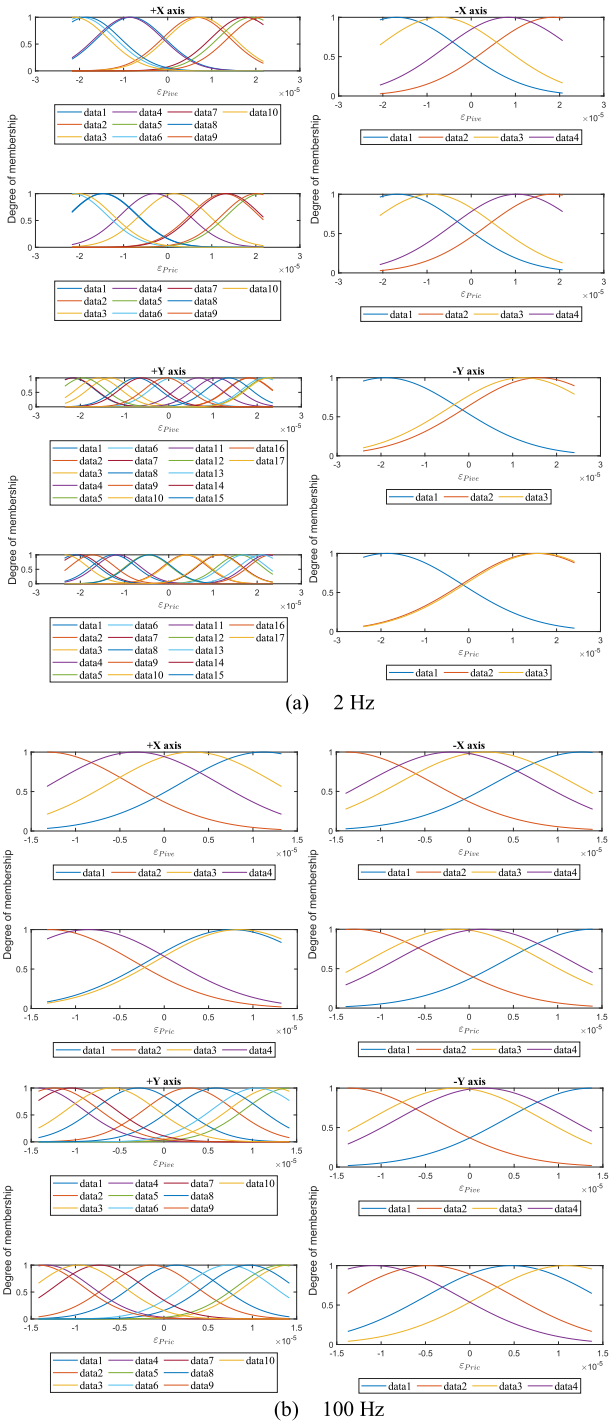

FIGURE 14. Input MFs of subtractive clustering-based DPPF's FISs.

Different nlhw models' structures were generated for the strain measurements at the Z-axis loading test's 3D force sensor beams. These estimators had different zeros and poles, different model structures, and different nonlinear functions, as shown in Table 3. A similar Hammerstein-Wiener model structure was used at 2 Hz and 10 Hz to achieve the best fit actual strain estimates from the piezoresistive element's

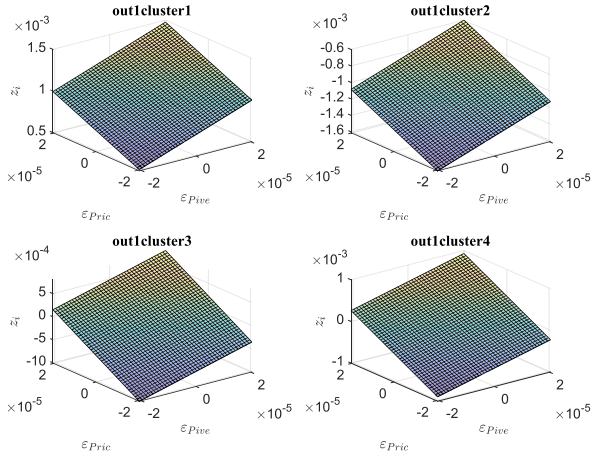

FIGURE 15. -X Beam output MFs under 2 Hz excitation for DPPF's FISs.

measurements. At 5 Hz strain estimate, a linear model was used with two zeros and three poles. At 100 Hz, the actual strain estimate was provided using the Wiener model. The piecewise linear function nonlinearity estimator was implemented at 2 Hz, 5 Hz, 10 Hz, and 100 Hz.

TABLE 3. THE NLHW models used at Z-loading strain estimation.

Test	Zeros	Poles	Model	Nonlinearity
Z 2HZ	3	4	Hammerstein-Wiener	pwlinear
Z 5HZ	2	3	linear	-
Z 10HZ	3	4	Hammerstein-Wiener	pwlinear
Z 100HZ	2	3	Wiener	pwlinear

The DPPF's FISs generated the desired piezoelectric and piezoresistive weights at the lower and higher frequencies, respectively. The FIS's output weights were recorded for each beam and at each frequency to analyze the DPPF's performance, as shown in Fig. 17. The total weight of one was assigned for piezoresistive and piezoelectric strain signals at 2 Hz, 5 Hz, 10 Hz, and 100 Hz, respectively. Relatively higher piezoelectric weights were assigned at 2 Hz and 10 Hz for the fused strain due to the presence of error presence at these frequencies. Conversely, the generated weights at 5 and 100 Hz were relatively less due to the accuracy of piezoresistive and piezoelectric sensors at these frequencies, respectively.

2) X AXIS LOADING SCENARIO

The DPPF's FISs for the X-axis scenario were produced using the same methodology utilized in the Z-axis scenario. The developed FISs' input MFs for the operating frequencies were retrieved at the X-axis loading test, as shown in Fig. 18 and Fig. 29. Please refer to the Appendix for the FISs' input MFs at 5 and 10 Hz under X loading conditions. Multiple FISs attained four MFs as their input variables, where the cluster influence ranges were assigned to be one. On the other hand, the highest number of inputs MFs was achieved at the +X-axis and +Y-axis FISs under excitation of 2 Hz, as shown in Fig. 18a. The cluster influence ranges for the FIS's piezoresistive and piezoelectric inputs' MFs at +Y beam (2 Hz) were 0.4 and 0.3, respectively, which resulted in 21 MFs. The output MFs and rule output levels were generated using the same procedure that was used for the Z-axis loading fusion. Each beam's FIS used the same set of rules in Table 2. However, the number of rules (n) used matched the same number of input/outputs MFs number.

Using the Simulink model, the generated DPPF's FISs were tested and analyzed in the X-axis loading scenario. The generated DPPF's fused strain, strain measurements, reference strain gauge measurements, and nlhw models' estimations were obtained and presented, as shown in Fig. 19. The DPPF method had merged both measurements and achieved accurately fused strain measurements. On the other hand, the nlhw models provided good actual strain estimates at most frequencies. Under the Z-axis loading test at 2 Hz, phase shifts were observed in both the piezoresistive and piezoelectric strain measurements compared to the strain gauges' measurement, as shown in Fig. 19a. These differences resulted from the variations in capacitances C1, used for the piezoresistive and piezoelectric circuits in both loading experiments. The sets of n rules used by each beam's FIS matched the same number of input/outputs MFs number.

As shown in Fig.19, the nlhw models produced perfect estimates for the strain measurements at the 3D force sensor's beams in the X-axis vibration experiment. The parameters used to generate these models are shown in Table 4. A Wiener model structure was used for the three highest frequencies, which achieved the best fit of actual strain estimates. The Wieners models utilized the piecewise linear function nonlinearity estimator as the structure output's nonlinear blocks. A linear model was used for strain estimate an excitation of 5 Hz with the highest number of zeros and poles of four and five, respectively. The same model Wiener model's structure was used for both the Z-axis and X-axis loading test under 100 Hz for the 3D force sensor's beams.

TABLE 4. The NLHW models used at X-loading strain estimation.

Test	Zeros	Poles	Model	Nonlinearity
X2HZ	4	5	linear	-
X5HZ	3	4	Wiener	pwlinear
X10HZ	3	4	Wiener	pwlinear
X100HZ	2	3	Wiener	pwlinear

The desired piezoelectric and piezoresistive weights were generated by the DPPF's FISs at the lower and higher frequencies, respectively. The output weights were retrieved to investigate the DPPF's performance in the fusion of every beam strain fusion, as shown in Fig. 20. Similar to the Z-axis loading characteristics' fusion, the piezoresistive strain signals at excitations of 2 Hz, 5 Hz, and 10 Hz were given a weight of one. On the other hand, the piezoelectric

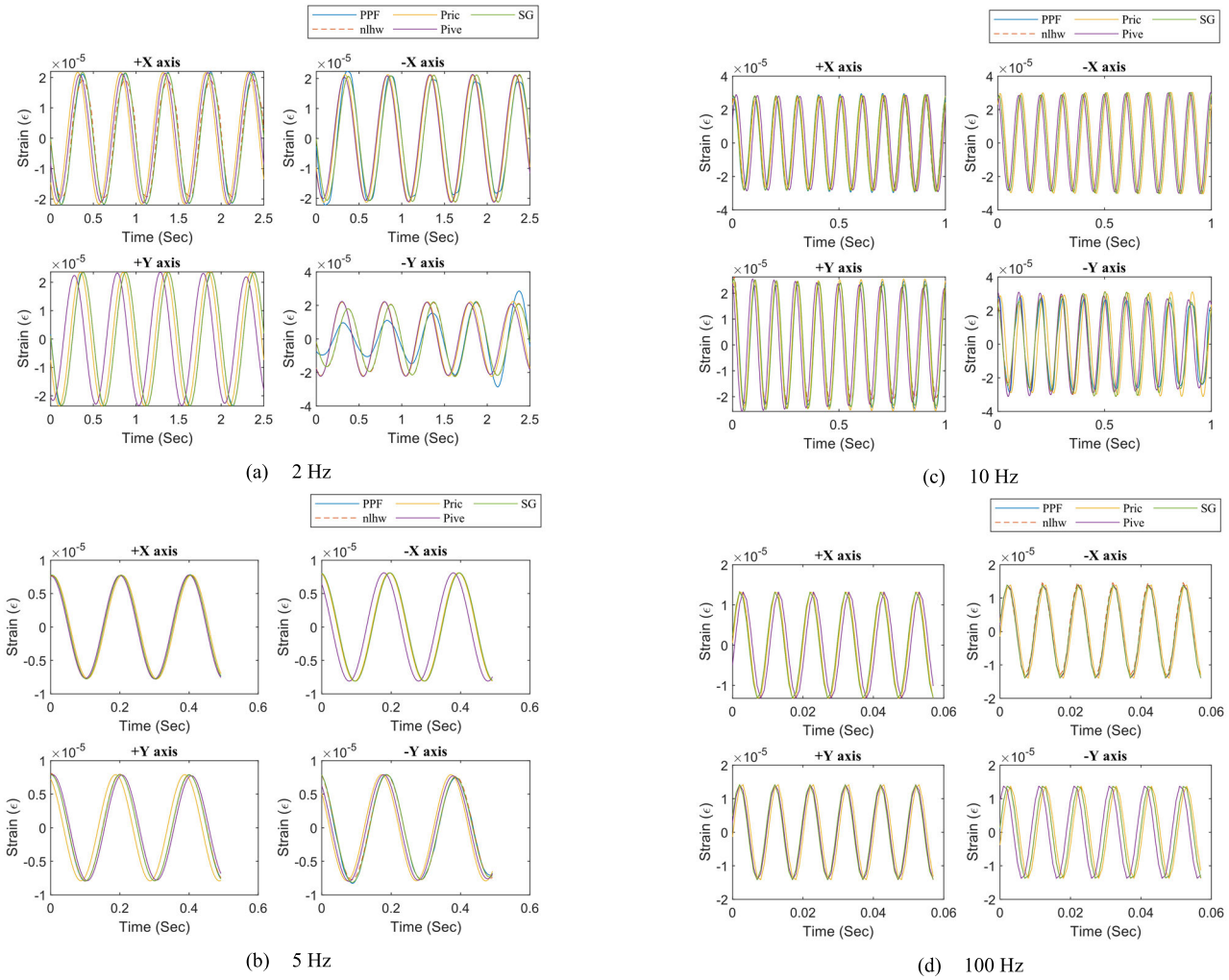

FIGURE 16. Z-axis loading results of the PPF.

element's measurements were accorded the total weights at 100 Hz vibration. The designed FIS produced higher weights at the 2 and 5 Hz frequencies due to the more significant inherited phase shift of the piezoresistive and piezoelectric strain measurement at the elastic structure's beams. Conversely, lower weights were assigned at the Y-axis beams because of the loading in the X direction and minimum strains' measurements at the Y-axis beams' sensing placements.

C. 3D FORCE SENSOR VIBRATION AND THE EPPF

The strain measurements were fused using a single FIS for a specific operating frequency. This method restricted the DPPF method from performing at a single frequency or local fusion. As a result, the EPPF was introduced to perform the fusion at a wide range of frequencies. The piezoresistive measurements were more reliable at the 2 Hz, 5 Hz, and 10 Hz frequencies than were the piezoelectric element's measurements. The EPPF's FIS fused strain measurement at these frequencies. The whole piezoresistive strain value was considered in Equation (6), while the FIS generated the needed weight to achieve accurately fused strain results. The EPPF was produced and tested only for the +X and +Y beams. Each beam was treated as a separate system of a singly supported beam. The previous piezoresistive, piezoelectric, and strain gauge measurement data obtained from the two-directional loading and three frequencies were cascaded for each beam separately. In this way, a single signal contained the three frequencies for each measurement at every loading scenario. These measurements were used to generate the EPPFs' FISs, from which their input MFs were retrieved, as shown in Fig. 21. A single FIS was generated for each set of directional loading experimental data. The +X beam's FISs had higher numbers of MFs compared to the +Y beam's FISs. Six input MFs were generated for the +Y beam from the Z-axis loading condition data, and four input MFs were generated for the +Y beam under the X-axis loading condition data. The output MFs and rule output levels were generated using the same method that was used in the Z-axis loading fusion.

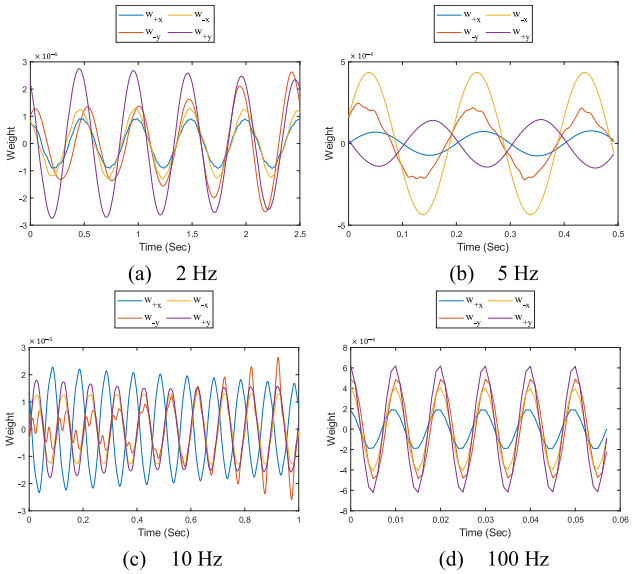

FIGURE 17. The DPPF's generated weights for piezoelectric and piezoresistive sensors at the Z-axis loading test.

The EPPF's MFs were investigated due to the notable difference in MFs number difference between +X and +Y beams. The clustering tool in MATLAB was used to identify and analyze the number of MFs in each of the four cases. The relationship and the clusters numbers were generated using the piezoresistive strain measurement, piezoelectric strain measurement, and the desired piezoelectric weight, as shown in Fig. 22. Only the cluster influence range was used to produce the EPPF's FISs, while other clustering parameters were kept at the default values. At the +X beam's FISs, three approximately concentric ellipses were used to represent the relationship between the piezoresistive strain, piezoelectric strain, and the piezoelectric sensor's weight. Each elliptical function corresponds to a particular frequency's desired piezoelectric weights. This correspondence required a higher number of clusters, leading to a more significant number of MFs required for more accurately fused strain values. Conversely, the interaction of two or more of these ellipses in for the +Y beam minimized the number of clusters needed to perform the fusion because one cluster or MF could be utilized for multiple frequencies' fusion. As shown in Fig. 22d, the smallest number of three MFs was assigned based on the given data due to the relatively smaller areas and high interfaces of these functions.

The generated EPPF's FISs were tested and analyzed in the 3D force sensor using the cascaded data and the validation Simulink model. The EPPF's fused strain was then compared with the piezoresistive and piezoelectric element's measurements, nlhw models estimates, and strain gauges measurements, as shown in Fig. 23. The EPPF's fused strains tracked well with the measurements from the reference strain gauges for the two beams in the Z-axis and X-axis loading experiments. Even though the original data was cascaded from the previous experiments, there were smooth transitions between

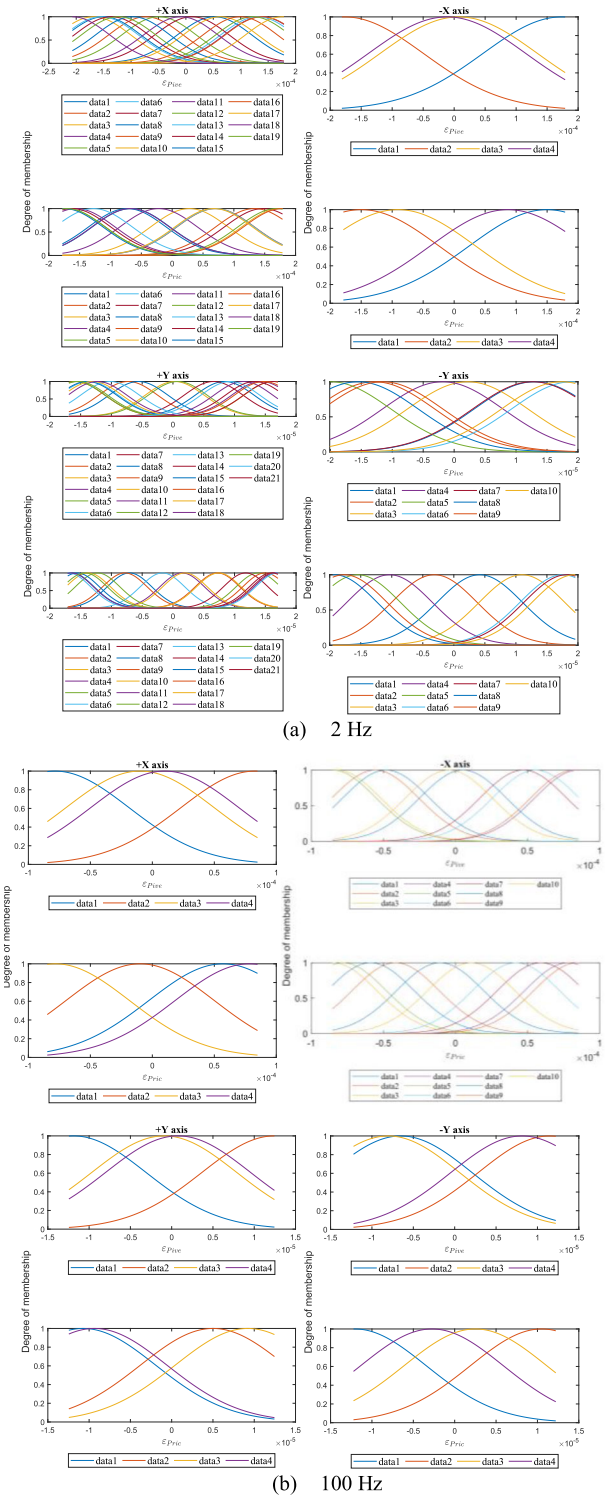

FIGURE 18. Input MFs of Subtractive clustering-based DPPF's FISs for X loading test.

the strain measurements through the different frequencies compared to the nlhw models.

The nlhw model produced good estimates for the actual strains using the piezoresistive element's measurements at each beam. The best actual strain estimates were

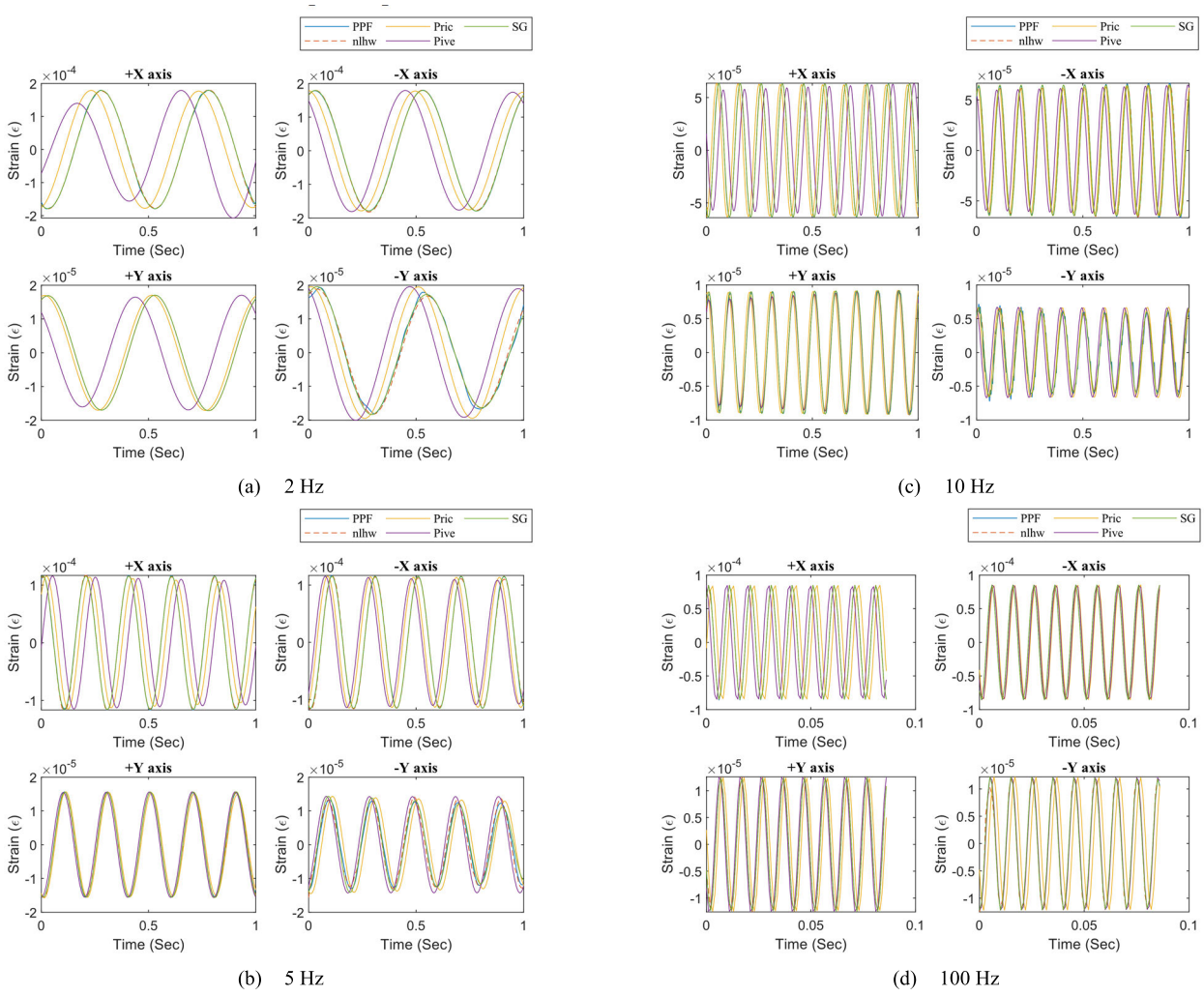

FIGURE 19. X-axis loading DPPF results.

reached using the nlhw model parameter shown in Table 5. The Hammerstein model was chosen for the estimate for all tests except at the X-axis loading of +Y beam, which instead used a linear model with 19 zeros and 20 poles. The input sigmoid network function was used for the Hammerstein model, which utilized 18 zeros and 19 poles.

TABLE 5. The NLHW models used at Z and X loading strain estimation using the cascaded data.

Test	Zeros	Poles	Model	Nonlinearity
+X beam (z)	18	19	Hammerstein	sigmoidnet
+X beam (x)	18	19	Hammerstein	sigmoidnet
+Y beam (z)	18	19	Hammerstein	sigmoidnet
+Y beam (x)	19	20	linear	-

The EPPF's FISs produced the desired piezoelectric weights for the accompanying measurements taken at different frequencies. The output weights were retrieved to analyze the EPPF's performance for +X beam's strain fusion and +Y beam's strain fusion, as shown in Fig. 24. The EPPF's generated weights were classified into three groups of different weight values. For the +X beam, three distinct weight values in both loading tests resulted in the higher MFs. By contrast, two similar weight groups with very close magnitude were observed in the +Y beam's tests, as shown in Fig 24c, d. Consequently, only a small number of MFs were needed, as shown in Fig 22c, d.

D. THE DPPF AND EPPF METHODS' RMSE COMPARED TO NLHW MODELS

The RMSE was used to assess the proposed fusion method's performance and to compare the results of the method with the actual estimate of the nonlinear models. For the DPPF method, the RMSE of the fused strain was calculated for the Z-axis and X-axis loading scenarios under the excitation

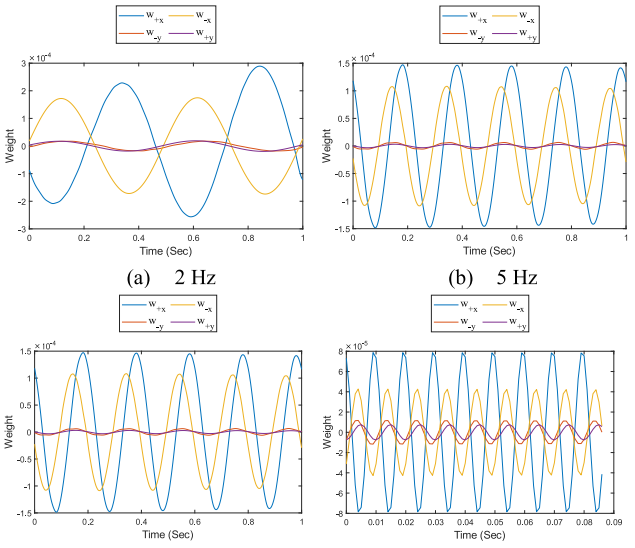

FIGURE 20. The DPPF's generated weights for piezoelectric and piezoresistive sensors at the X-axis loading test.

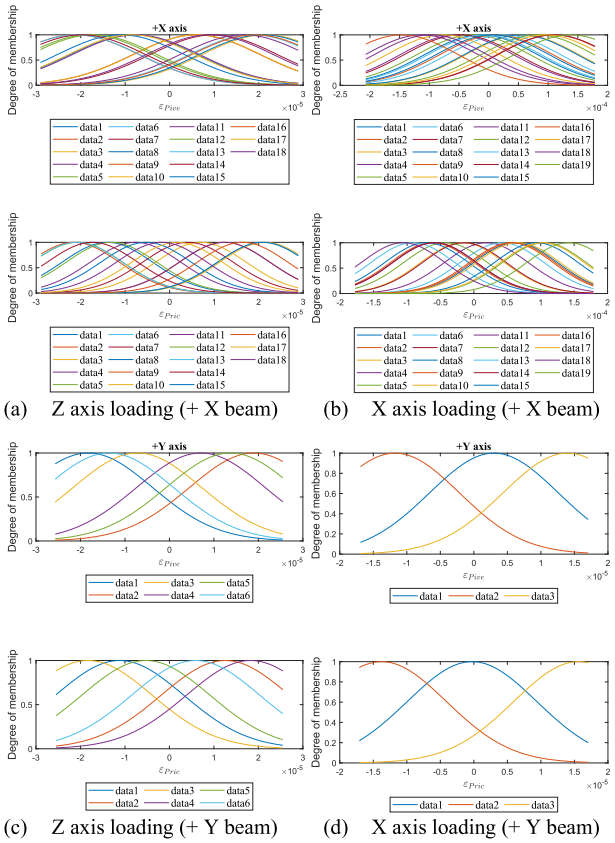

FIGURE 21. Input MFs of the EPPF's FISs for the +X and +Y beams.

frequencies of 2 Hz, 5 Hz, 10 Hz, and 100 Hz, as shown in Fig. 25 and Fig. 26. The DPPF method achieved the smallest RMSE under most of the loading's directions and frequencies compared to the nlhw models. However, higher RMSEs were associated with -Y beams at 2 Hz and 10 HZ excitations

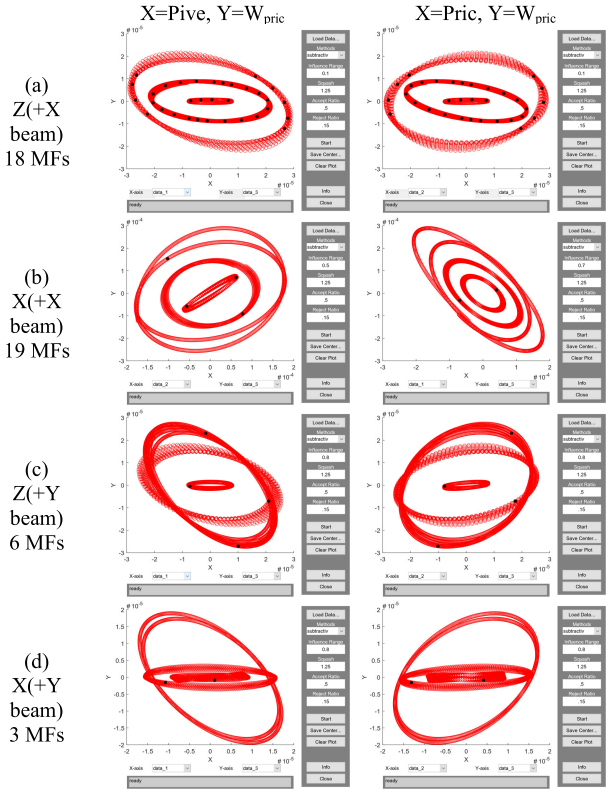

FIGURE 22. EPPF number of MFs and clusters investigation.

of Z-axis loading experiments. This is because of an issue with the -Y-axis strain gauge circuit, which had a circuit element failure or external noise, affecting the actual strain measurement. When an actual strain measurement was used to generate and tune the fusion FISs.

The cumulative DPPF fused strains' RMSEs at all frequencies were lower than the nlhw models' RMSE by 34%, 33%, and 13% at the +X-axis, -X-axis, and +Y-axis beams, respectively. On the other hand, the nlhw models estimated the strain at a 60.8% lower cumulative RMSE compared to the proposed fusion method because of the influence of the noise strain gauge at that beam. Relatively smaller RMSEs were perceived in the Z-axis loading test under the excitation of 2 Hz and 100 Hz. The DPPF achieved the smallest RMSE of 1E-10 at the +Y-axis beam under the vibration of 100 Hz.

Similarly, the EPPF method was analyzed and compared with nlhw models' strain estimate using the RMSE for the +X-axis beam and + Y beam under the two loading experiments, as shown in Fig. 27. The EPPF fused strains RMSE was lower during these testing scenarios except for the X-axis loading test of the +X-axis beam. This was due to the higher number of MFs needed to achieve more accurate fusion at that condition. The EPPF fused strain measurement achieved approximately 15% less accumulative RMSE compared to the nonlinear model. Relatively higher RMSEs were observed in the +X-axis beam under X-direction vibration due to the need for higher-order nlhw models and EPPF's MFs.

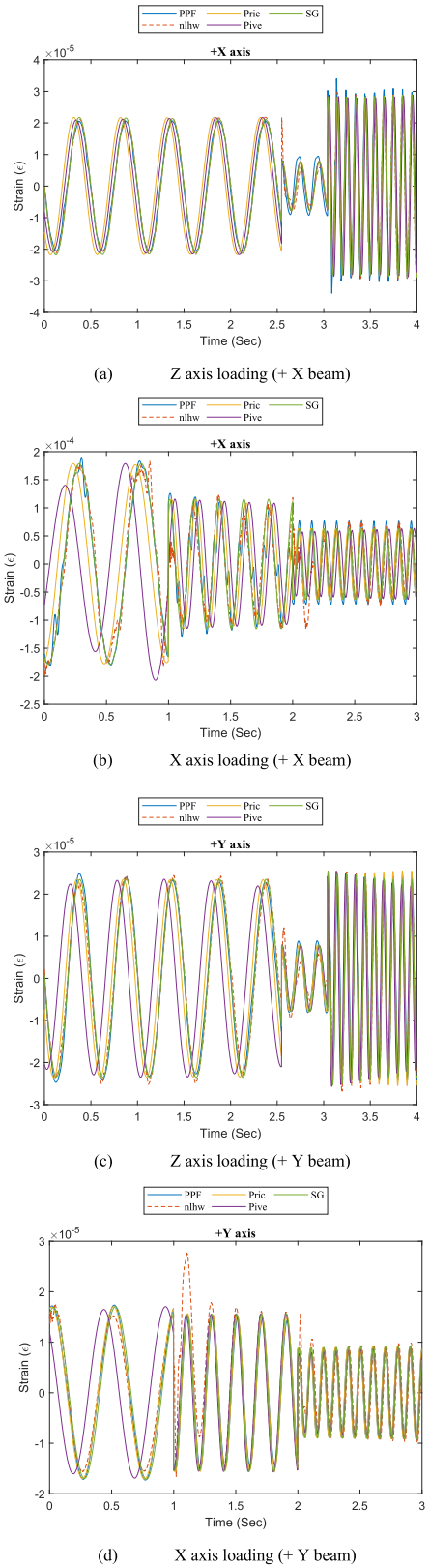

(a) Z axis loading (+ X beam)

(b) X axis loading (+ X beam)

(c) Z axis loading (+ Y beam)

(d) X axis loading (+ Y beam)

FIGURE 23. The EPPF results at the +X and +Y beams.

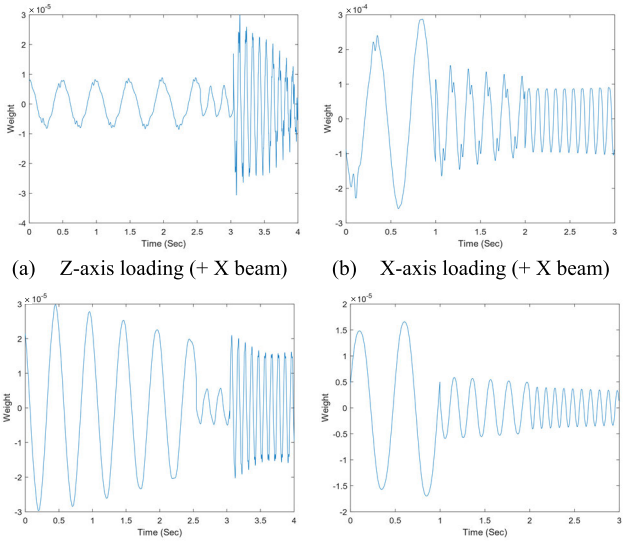

(a) Z-axis loading (+ X beam)

(b) X-axis loading (+ X beam)

(c) Z-axis loading (+ Y beam)

(d) X-axis loading (+ Y beam)

FIGURE 24. The generated EPPF's piezoelectric weight for +X and +Y beams.

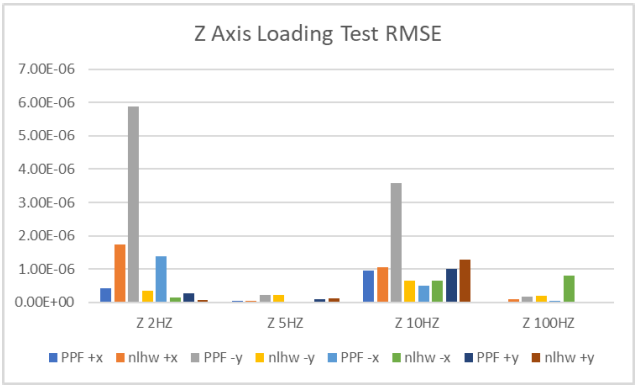

FIGURE 25. The DPPF and nlhw's models' RMSE at the Z-axis loading test.

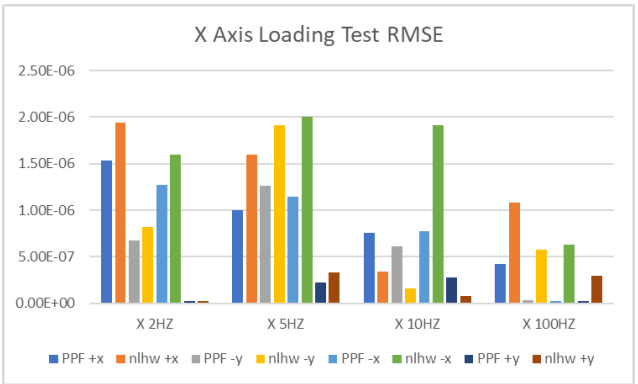

FIGURE 26. The DPPF and nlhw's models' RMSE at the X-axis loading test.

These results prove the capability of the proposed DPPF and EPPF to fuse the MWCNT/PVDF strain sensors' piezoresistive and piezoelectric measurements. The fused strains successfully matched the actual strains with minimal RMSEs at the 3D force sensor's structure using both the piezoresistive and piezoelectric characteristics. In the DPPF method, a single FIS merged the measurements based on their sensitivity at

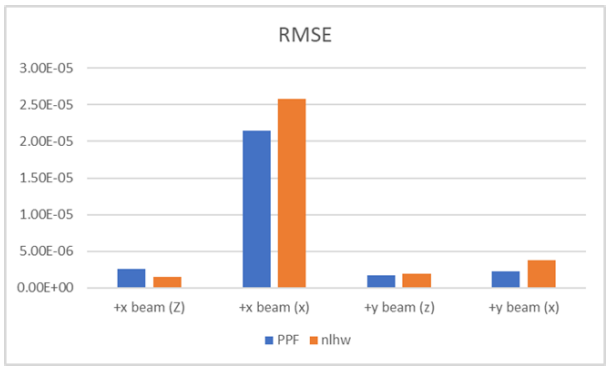

FIGURE 27. The EPPF and nlhw's models' RMSE.

a specific operating frequency, while single FISs were used to perform the fusion at a range of operating frequencies using the EPPF method.

VI. CONCLUSION

The MWCNT/PVDF nanocomposite films have been used in several strain sensing applications. They form a unique sensing element that can capture static/slow and dynamic strain measurements using their piezoresistive and piezoelectric characteristics, respectively. That led to limited strain measurements depending on the used characteristic and operating frequency. As a result, new fusion methods were introduced to combine the piezoresistive and piezoelectric element's measurements using the FL and subtractive clustering technique. The in situ 0.1 wt. and 2 wt.% MWCNT/PVDF strain sensors were fabricated using a spray-coating process and were chosen for piezoelectric and piezoresistive strain measurements, respectively. The sensitivity and accuracy of each characteristic were investigated using a supported beam under different excitation frequencies. The MWCNT/PVDF sensor was found to be sensitive at frequencies lower than 100 Hz, and more noise was observed at high frequencies. At the same time, the piezoelectric characteristic was found to be sensitive and contained less noise at the higher frequencies of 100 and 1000 Hz. However, the piezoelectric measurement was found not sensitive at very low frequencies. The 3D force sensor was introduced and used the fabricated strain sensing elements on its structure. The piezoresistive and piezoelectric films were attached at each beam, and reference strain gauges were attached on the opposite side for comparison and fusion method generation. Wheatstone bridge circuits were used for the piezoresistive sensors and strain gauges. By a charge amplifier circuit was used for the piezoelectric characteristic measurements. The 3D force sensor was excited at different operating frequencies in the Z-axis and the X-axis directions, while the 3D force sensor was assumed to perform similarly in the X-direction and Y-direction. The piezoresistive, piezoelectric, and strain gauges' measurements were used to generate the proposed DPPF and EPPF using the Fuzzy Logic and Global Optimization Toolboxes in MATLAB. These methods utilized the Sugeno FIS and the subtractive clustering technique to fuse the piezoresistive and piezoelectric measurements. Fusion

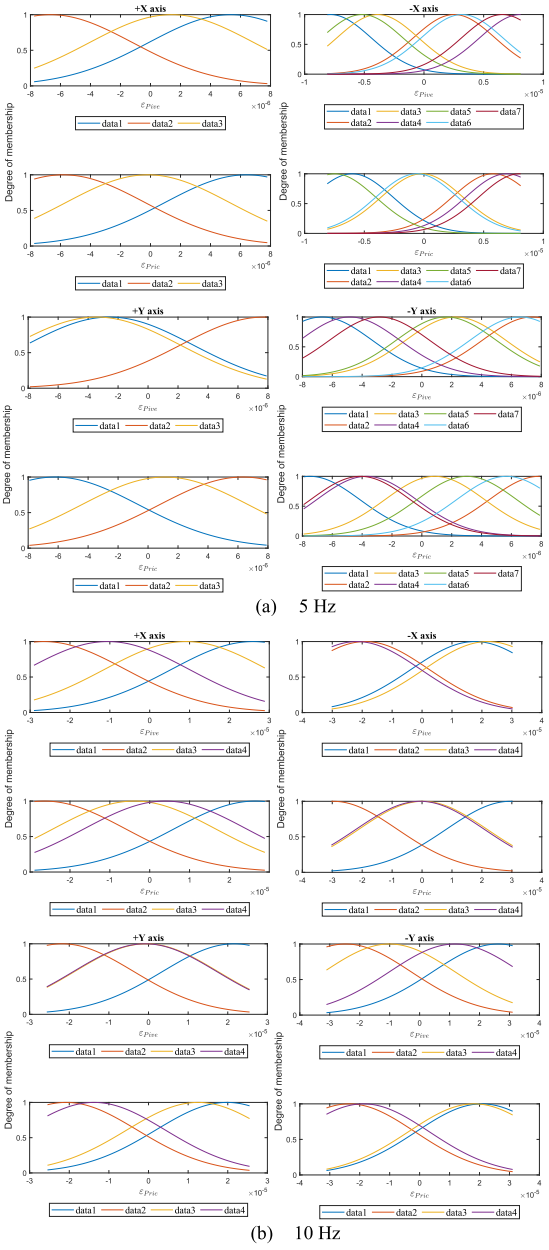

FIGURE 28. Input MFs of subtractive clustering-based DPPF's FISs for Z loading test.

was successfully performed at a single operating frequency using a single FIS in the DPPF method, while the EPPF method accurately fused both characteristics at the range of operating frequencies using a unique FIS. The method achieved a lower RMSE value compared to different nlhw actual strain estimation models. The findings of this study indicate that the MWCNT/PVDF measurement characteristics can be fused using the DPPF and EPPF methods and achieve a wide band strain sensor. However, the proposed fusion method is not restricted to strain measurements, but rather has the potential to fuse different measurements for a single phenomenon, where particular limitations restrict measurement characteristics.

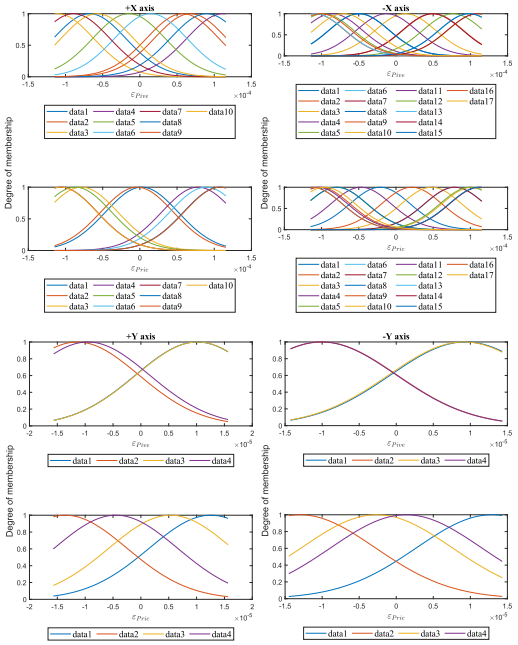

(a) 5 Hz

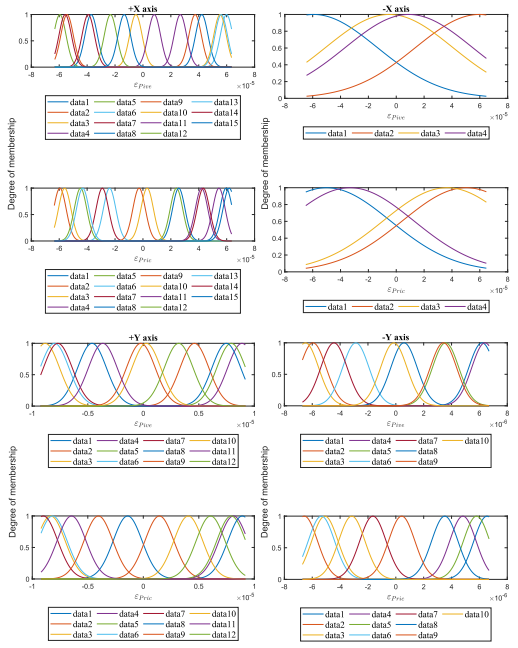

(b) 10 Hz

FIGURE 29. Input MFs of subtractive clustering-based DPPF's FISs for X loading test.

Further work needs to be performed to establish whether the proposed fusion method applies to different signal types and shapes. Our results are promising and should be validated using a more frequency investigation on the MWCNT/PVDF piezoresistive and piezoelectric characteristics. A stack of piezoresistive and piezoelectric layers will result in a smaller sensing attachment space to improve the NC sensor structure. We believe that our research will serve as a base for future studies on NC measurement fusion.

APPENDIX

See Figures 28 and 29.

ACKNOWLEDGMENT

The authors would like to thank the Integrated Nanosystems Development Institute (INDI), Indiana University–Purdue University Indianapolis for their support and guidance in the fabrication process of the nanocomposite films.

REFERENCES

[1] A. Song and L. Fu, "Multi-dimensional force sensor for haptic interaction: A review," *Virtual Reality Intell. Hardw.*, vol. 1, no. 2, pp. 121–135, Jan. 2019.

[2] U. Seibold, B. Kubler, and G. Hirzinger, "Prototype of instrument for minimally invasive surgery with 6-axis force sensing capability," in *Proc. IEEE Int. Conf. Robot. Automat.*, Apr. 2005, pp. 496–501.

[3] Q. Liang, D. Zhang, W. Wu, and K. Zou, "Methods and research for multi-component cutting force sensing devices and approaches in machining," *Sensors*, vol. 16, no. 11, p. 1926, 2016.

[4] R. A. Brookhuis, T. S. J. Lammerink, R. J. Wiegerink, M. J. de Boer, and M. C. Elwenspoek, "3D force sensor for biomechanical applications," *Sens. Actuators A, Phys.*, vol. 182, pp. 28–33, Aug. 2012.

[5] M.-K. Kang, S. Lee, and J.-H. Kim, "Shape optimization of a mechanically decoupled six-axis force/torque sensor," *Sens. Actuators A, Phys.*, vol. 209, pp. 41–51, Mar. 2014.

[6] Y. Lu, L. Chen, P. Wang, B. Zhang, Y. Zhao, and B. Hu, "Statics and stiffness analysis of a novel six-component force/torque sensor with 3-RPPS compliant parallel structure," *Mech. Mach. Theory*, vol. 62, pp. 99–111, Apr. 2013.

[7] Y. Hou, D. Zeng, J. Yao, K. Kang, L. Lu, and Y. Zhao, "Optimal design of a hyperstatic stewart platform-based force/torque sensor with genetic algorithms," *Mechatronics*, vol. 19, no. 2, pp. 199–204, Mar. 2009.

[8] A. M. Alotaibi and S. Anwar, "Analysis of bio-inspired structures for 3D force sensing using virtual prototyping," *Biomed. Biotechnol. Eng.*, vol. 59407, Nov. 2019, Art. no. V003T04A074.

[9] H. Alam, D. Soetraprawata, and Bahrudin, "The structural design of six-axis force/torque sensor using virtual prototyping technique," *J. Sci. Res. Rep.*, vol. 5, no. 2, pp. 120–131, Jan. 2015.

[10] J. Yao, H. Zhang, X. Xiang, H. Bai, and Y. Zhao, "A 3-D printed redundant six-component force sensor with eight parallel limbs," *Sens. Actuators A, Phys.*, vol. 247, pp. 90–97, Aug. 2016.

[11] Y.-J. Li, G.-C. Wang, D. Zhao, X. Sun, and Q.-H. Fang, "Research on a novel parallel spoke piezoelectric 6-DOF heavy force/torque sensor," *Mech. Syst. Signal Process.*, vol. 36, no. 1, pp. 152–167, Mar. 2013.

[12] Y. Noh, J. Bimbo, S. Sareh, H. Wurdemann, J. Fraś, D. Chathuranga, H. Liu, J. Housden, K. Althoefer, and K. Rhode, "Multi-axis force/torque sensor based on simply-supported beam and optoelectronics," *Sensors*, vol. 16, no. 11, p. 1936, 2016.

[13] U. Kim, D.-H. Lee, Y. B. Kim, D.-Y. Seok, and H. R. Choi, "A novel six-axis force/torque sensor for robotic applications," *IEEE/ASME Trans. Mechatronics*, vol. 22, no. 3, pp. 1381–1391, Jun. 2017.

[14] R. K. Singh, S. W. Lye, and J. Miao, "PVDF nanofiber sensor for vibration measurement in a string," *Sensors*, vol. 19, no. 17, p. 3739, Aug. 2019, doi: 10.3390/s19173739.

[15] W. Chen, P. Yang, W. Shen, C. Zhu, D. Lv, R. Tan, and W. Song, "Flexible room temperature ammonia gas sensor based on in suit polymerized PANI/PVDF porous composite film," *J. Mater. Sci., Mater. Electron.*, vol. 31, no. 14, pp. 11870–11877, Jul. 2020, doi: 10.1007/s10854-020-03741-9.

[16] R. Guo, H. Zhang, S. Cao, X. Cui, Z. Yan, and S. Sang, "A self-powered stretchable sensor fabricated by serpentine PVDF film for multiple dynamic monitoring," *Mater. Des.*, vol. 182, Nov. 2019, Art. no. 108025, doi: 10.1016/j.matdes.2019.108025.

[17] K. Kim, J. Park, J.-H. Suh, M. Kim, Y. Jeong, and I. Park, "3D printing of multiaxial force sensors using carbon nanotube (CNT)/thermoplastic polyurethane (TPU) filaments," *Sens. Actuators A, Phys.*, vol. 263, pp. 493–500, Aug. 2017.

[18] C. C. Su, T. Liu, N. K. Chang, B. R. Wang, and S. H. Chang, "Two dimensional carbon nanotube based strain sensor," *Sens. Actuators A, Phys.*, vol. 176, pp. 124–129, Apr. 2012.
[19] S. S. Park, K. Parmar, S. Shajari, and M. Sanati, "Polymeric carbon nanotube nanocomposite-based force sensors," *CIRP Ann.*, vol. 65, no. 1, pp. 361–364, 2016.
[20] M. B. Bryning, M. F. Islam, J. M. Kikkawa, and A. G. Yodh, "Very low conductivity threshold in bulk isotropic single-walled carbon nanotube-epoxy composites," *Adv. Mater.*, vol. 17, no. 9, pp. 1186–1191, May 2005.
[21] G. T. Pham, "Characterization and modeling of piezoresistive properties of carbon nanotube-based conductive polymer composites," Florida State Univ., Tallahassee, FL, USA, Tech. Rep. 3348527, 2008.
[22] Alamusi, N. Hu, H. Fukunaga, S. Atobe, Y. Liu, and J. Li, "Piezoresistive strain sensors made from carbon nanotubes based polymer nanocomposites," *Sensors*, vol. 11, no. 11, pp. 10691–10723, 2011.
[23] B. Hu, N. Hu, Y. Li, K. Akagi, W. Yuan, T. Watanabe, and Y. Cai, "Multi-scale numerical simulations on piezoresistivity of CNT/polymer nanocomposites," *Nanosc. Res. Lett.*, vol. 7, no. 1, pp. 1–11, Dec. 2012.
[24] C. Li, E. T. Thostenson, and T.-W. Chou, "Dominant role of tunneling resistance in the electrical conductivity of carbon nanotube–based composites," *Appl. Phys. Lett.*, vol. 91, no. 22, Nov. 2007, Art. no. 223114.
[25] C. Sun, J. Shi, D. J. Bayerl, and X. Wang, "PVDF microbelts for harvesting energy from respiration," *Energy Environ. Sci.*, vol. 4, no. 11, p. 4508, 2011.
[26] D. He, W. Liu, Y. Ruan, X. Fu, and C. Stefanini, "Preliminary study on piezoresistive and piezoelectric properties of a double-layer soft material for tactile sensing," *Mater. Sci.*, vol. 21, no. 2, pp. 238–243, Jun. 2015, doi: 10.5755/j01.ms.21.2.6454.
[27] S. Khan, W. Dang, L. Lorenzelli, and R. Dahiya, "Flexible pressure sensors based on screen-printed P(VDF-TrFE) and P(VDF-TrFE)/MWCNTs," *IEEE Trans. Semicond. Manuf.*, vol. 28, no. 4, pp. 486–493, Nov. 2015, doi: 10.1109/tsm.2015.2468053.
[28] M. Sanati, A. Sandwell, H. Mostaghimi, and S. Park, "Development of nanocomposite-based strain sensor with piezoelectric and piezoresistive properties," *Sensors*, vol. 18, no. 11, p. 3789, Nov. 2018, doi: 10.3390/s18113789.
[29] A. Alotaibi and S. Anwar, "A fuzzy logic based piezoresistive/piezoelectric fusion algorithm for carbon nanocomposite wide band strain sensor," *IEEE Access*, vol. 9, pp. 14752–14764, 2021.
[30] Space for Life. *Top View of the Ideal Structure*. Accessed: Jun. 1, 2021. [Online]. Available: http://m.espacepourlavie.ca/en/file/6735
[31] R. Figliola and D. Beasley, *Theory and Design for Mechanical Measurements*. New York, NY, USA: Wiley, 2001.
[32] *INA333 Data Sheet, Product Information and Support | TI.com*, document INA333. Accessed: Jun. 27, 2021. [Online]. Available: https://www.ti.com/product/INA333
[33] *REF5025 Data Sheet, Product Information and Support | TI.com*, document REF5025. Accessed: Jun. 27, 2021. [Online]. Available: https://www.ti.com/product/REF5025
[34] A. V. Shirinov and W. K. Schomburg, "Pressure sensor from a PVDF film," *Sens. Actuators A, Phys.*, vol. 142, no. 1, pp. 48–55, 2008.
[35] T. Ross, *Fuzzy Logic With Engineering Applications*, 4th ed. Hoboken, NJ, USA: Wiley, 2017.
[36] C. Lee, "Fuzzy logic in control systems: Fuzzy logic controller. I and II," *IEEE Trans. Syst., Man, Cybern.*, vol. 20, no. 2, pp. 404–418, Mar./Apr. 1990, doi: 10.1109/21.52551.
[37] M. Sugeno, "An introductory survey of fuzzy control," *Inf. Sci.*, vol. 36, nos. 1–2, pp. 59–83, 1985. Accessed: Oct. 18, 2020, doi: 10.1016/0020-0255(85)90026-x.
[38] Mathworks. (2020). *Sugeno Fuzzy Inference System—MATLAB*. Accessed: Oct. 18, 2020. [Online]. Available: https://www.mathworks.com/help/fuzzy/sugfis.html
[39] *MATLAB Version 9.7.0.1296695 (R2019b) Update 4*, MathWorks, Natick, MA, USA, 2010.
[40] Z. Ounaies, C. Park, K. E. Wise, E. J. Siochi, and J. S. Harrison, "Electrical properties of single wall carbon nanotube reinforced polyimide composites," *Compos. Sci. Technol.*, vol. 63, no. 11, pp. 1637–1646, Aug. 2003.
[41] C. H. Hu, C. H. Liu, L. Z. Chen, and S. S. Fan, "Semiconductor behaviors of low loading multiwall carbon nanotube/poly(dimethylsiloxane) composites," *Appl. Phys. Lett.*, vol. 95, no. 10, Sep. 2009, Art. no. 103103.
[42] A. A. Sahraei, M. Ayati, M. Baniassadi, D. Rodrigue, M. Baghani, and Y. Abdi, "AC and DC electrical behavior of MWCNT/epoxy nanocomposite near percolation threshold: Equivalent circuits and percolation limits," *J. Appl. Phys.*, vol. 123, no. 10, Mar. 2018, Art. no. 105109.
[43] N. Hu, Y. Karube, C. Yan, Z. Masuda, and H. Fukunaga, "Tunneling effect in a polymer/carbon nanotube nanocomposite strain sensor," *Acta Mater.*, vol. 56, no. 13, pp. 2929–2936, Aug. 2008.
[44] N. Shehata, E. Elnabawy, M. Abdelkader, A. Hassanin, M. Salah, R. Nair, and S. A. Bhat, "Static-aligned piezoelectric poly (Vinylidene Fluoride) electrospun nanofibers/MWCNT composite membrane: Facile method," *Polymers*, vol. 10, no. 9, p. 965, Sep. 2018.
[45] A. M. Vinogradov, S. C. Schumacher, and E. M. Rassi, "Dynamic response of the piezoelectric polymer PVDF," *Int. J. Appl. Electromagn. Mech.*, vol. 22, nos. 1–2, pp. 39–51, Oct. 2005.
[46] System Identification Toolbox Documentation. *System Identification Toolbox*. Accessed: Jun. 27, 2021. [Online]. Available: https://www.mathworks.com/help/ident/index.html
[47] Mathworks. (2020). *Sugeno Fuzzy Inference System—MATLAB*. Accessed: Jun. 18, 2021. [Online]. Available: https://www.mathworks.com/help/fuzzy/types-of-fuzzy-inference-systems.html
[48] M. Sugeno, *Industrial Applications of Fuzzy Control*. Amsterdam, The Netherlands: North-Holland, 1992.

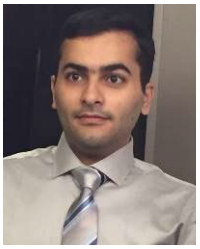

AHMED ALOTAIBI received the B.S. degree in mechanical engineering (mechatronics) from Taif University, Saudi Arabia, and the M.S. and Ph.D. degrees in mechanical engineering from Purdue University, West Lafayette, IN, USA. He is currently working as an Assistant Professor at the School of Mechanical Engineering, Taif University. His research interests center around the mechatronics and physical therapy tools instrumentation. His current research interest includes development of polymer nanocomposite-based wide band strain sensor for 3D force measurement using piezoelectric and piezoresistive data fusion.

SOHEL ANWAR (Member, IEEE) received the Ph.D. degree from The University of Arizona, Tucson, AZ, USA, in 1995. From 1995 to 1999, he worked as a Research and Development Engineer at Caterpillar, Inc., where he focused on X-By-Wire systems design for wheeled loaders. In 1999, he joined Ford Motor Company/Visteon Corporation as a Senior Research and Development Engineer, where he led the fault tolerant design of drive-by-wire systems. In 2004, he joined the Purdue School of Engineering and Technology, Indiana University Purdue University at Indianapolis (IUPUI). He is currently a Professor with the Department of Mechanical and Energy Engineering, Purdue School of Engineering and Technology, IUPUI. He is also the Director of the Mechatronics and Autonomous Research Laboratory (MARL). He has over 26 years of combined academic and industry research and development experience in the general area of mechatronics and controls. He has published over 150 papers in peer-reviewed journals and conference proceedings. He is also an inventor or a co-inventor on 14 U.S. patents. He is a member of ASME and a Faculty Advisor of SAE student chapter at IUPUI. He is on the editorial board of three international journals.